CrossMark

J. Fluid Mech. (2016), *vol.* 793, *pp.* 380–413. © Cambridge University Press 2016
doi:10.1017/jfm.2016.121

Layers and internal waves in uniformly stratified fluids stirred by vertical grids

S. A. Thorpe†

School of Ocean Sciences, Bangor University, Menai Bridge, Anglesey LL59 5AB, UK

(Received 20 April 2015; revised 7 January 2016; accepted 10 February 2016;
first published online 16 March 2016)

Laboratory experiments in which uniformly stratified fluids are stirred by horizontally moving vertical grids, or arrays of vertical rods, are reviewed to examine their consistency and to compare their findings, particularly those relating to the generation of layers. Selected experiments are of three types, those in which (*a*) turbulence spreads from a horizontally confined region where it is continuously generated by an oscillating grid; (*b*) grid stirring is maintained throughout a rectangular tank; or (*c*) a 'cloud' of turbulence decays after a short period of horizontally localized grid mixing. In all the experiments turbulence is generated over the full vertical extent of the tank. In the experiments of types (*a*) and (*c*) layers of comparable scale are observed to intrude into the ambient fluid from the turbulent region. In the type (*b*) experiments, layers form only when the time interval between the passage of the grid through the stratified fluid is sufficiently long, allowing turbulence to decay substantially between grid strokes. Two mechanisms are found to be dominant in the production of layers. In experiments of type (*a*) and (*c*) overturning eddies in the turbulent region of scale significantly larger than the Ozmidov length scale collapse and spread, intruding and forming layers in the adjoining laminar region. Internal shear waves propagating ahead of the intrusions have a vertical wavelength that is approximately twice the layer height. In type (*b*) experiments, layers are formed through a process described by Holford & Linden (*Dyn. Atmos. Oceans*, vol. 30, 1999*a*, pp. 173–198): the bending of vortices shed by the grid bars. The height of the layers is approximately half the vertical wavelength of internal shear waves that travel at the speed of the grid. It is proposed that the flow field of the shear waves bends the vortices, resulting in diapycnal mixing that forms the layers. The relationship of layers and internal shear waves in the experiments is therefore as follows: in type (*a*) and (*c*) experiments internal waves are generated by layers intruding from the turbulent region into the quiescent stratified region, but in experiments of type (*b*) internal waves drive and dictate the height of the layers; layers are generated as a consequence of vortex bending by internal waves. There is insufficient evidence to establish whether zigzag instability, either of vortex pairs or of vortex streets shed by a moving grid, accounts for the layers in any of the three types of grid experiments. The Phillips and Posmentier instability may reinforce layers formed by other processes. The generation of pancake vortices or vortical mode motion is left for later review.

Key words: stratified turbulence, turbulent mixing, wave–turbulence interactions

† Address for correspondence: 1A, Green Edge, Beaumaris, Anglesey LL58 8BY, UK.
Email address for correspondence: oss413@bangor.ac.uk

https://doi.org/10.1017/jfm.2016.121 Published online by Cambridge University Press

1. Introduction

1.1. *Turbulence and layers*

The effect and properties of turbulence in a stratified fluid are of fundamental importance in the study of environmental fluid dynamics. In the hope of clarifying the basic physical processes, numerous laboratory experiments have been made and reported in which turbulence is generated in stratified fluids by moving grids spanning the width and depth of a laboratory tank. By some yet undetermined means, turbulence sometimes leads to the formation of multiple horizontal layers of relatively uniform density within a fluid that, initially, is uniformly stratified (i.e. of constant buoyancy frequency, N). As sketched in figure 1, the layers occur in three different types of experiment, (*a–c*), in which vertical grids move horizontally through the uniformly stratified fluid. In type (*a*), intrusive layers spread from a horizontally localised region where it is continuously generated by a grid oscillating with frequency, ω, typically $\sim 10N$. The grid may be located at the end of a tank as in figure 1(*a*) or in the centre as in figure 2. In type (*b*) experiments the grid moves at constant speed, U, back and forth throughout the length of a rectangular tank with relatively lower frequency $\omega \sim 0.1N$. Layers are apparent when the grid motion is temporally stopped. In type (*c*) experiments a 'cloud' of turbulence decays after a short period of horizontally localized grid mixing. Layers develop as intrusions from the turbulent cloud. The layers in some of the experiments are sometimes remarkably uniform and periodic in the vertical, e.g. as observed in type (*a*) experiments by Browand, Guyomar & Yoon (1987; see especially their figure 15) or in type (*b*) experiments by Ruddick, Mcdougall & Turner (1989, figure 4*d*). Internal waves are observed to propagate ahead of the intrusions in experiments of type (*a*) and (*c*). Horizontal 'pancake' vortices related to the generation vortical modes are found in the late stages of some experiments (see e.g. Praud, Fincham & Sommeria 2005), but are left for consideration elsewhere.

Our purpose is, by synthesising and comparing existing laboratory and numerical studies, to examine the possible mechanisms that produce layers and to explain their vertical scale. The formation of layers by turbulence has attracted the attention of oceanographers seeking to explain the fine-scale density structure of the ocean. Whilst single layers are formed by the diapycnal mixing of a breaking internal wave, several mechanisms (including double-diffusive convection; Turner 1973) are known to cause multiple layers. Layers form as intrusions (Manins 1976) from a density current flowing down a sloping boundary (e.g. Baines 2001; Snow & Sutherland 2014). They may also be caused by turbulent mixing on a slope (Thorpe 1998; the vertical size of layers observed by Inall (2009) in Loch Etive, Scotland, appears, however, to be associated with the scale of roughness on an adjoining slope rather than with that of turbulence, e.g. the Ozmidov overturning scale, on a uniform slope). Layers are sometimes transient, moving vertically through the density field, a consequence of internal wave packets propagating through and straining a background density (e.g. Lazier 1973; Alford & Gregg 2001). Whilst yet to be observed either in the laboratory or in the natural environment, layers might also be formed by the successive breaking of internal waves in a wave group as it propagates upwards or downwards through a stratified environment (Thorpe 1999). Although ostensibly the fluid motions and layers produced by a grid in the laboratory have little immediate relevance to the ocean (or to lakes or the atmosphere), the grid experiments offer information about the time scale and nature of the collapse of turbulence and provide insight into processes that may act in the natural environment. A relationship between layers and internal waves may be the most significant common factor.

https://doi.org/10.1017/jfm.2016.121 Published online by Cambridge University Press

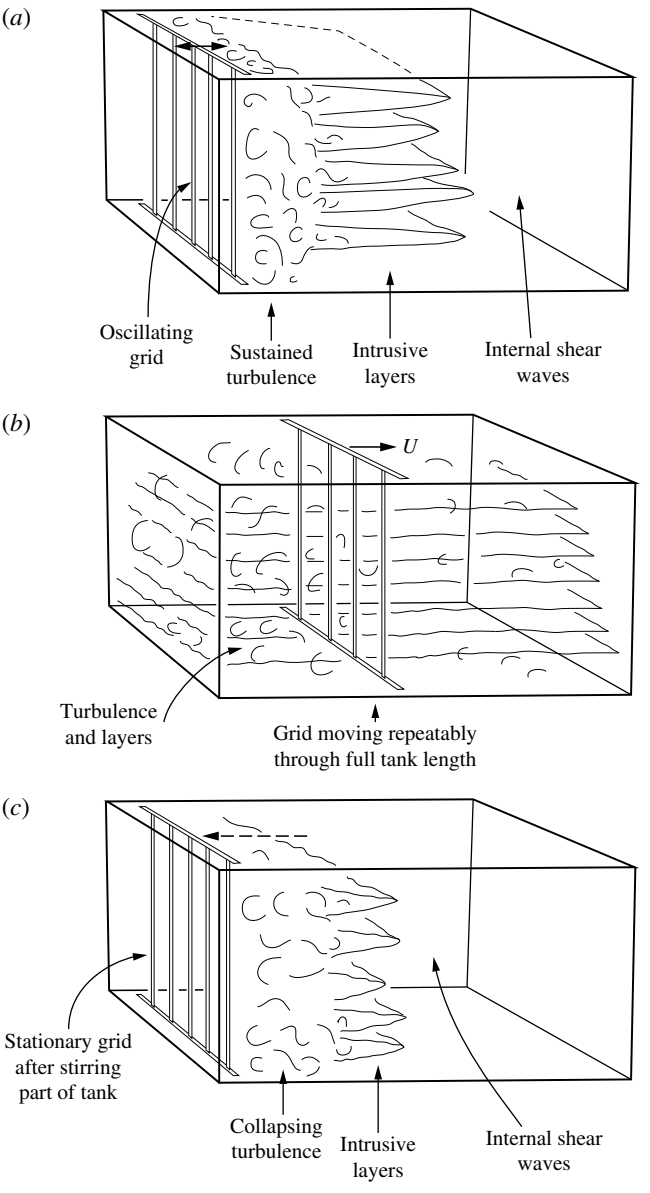


FIGURE 1. A sketch of layers formed in the three types of laboratory experiments, (*a–c*). In (*a*) the grid oscillates sinusoidally with amplitude much less than the tank length and with frequency much exceeding the buoyancy frequency, N. In (*b*) the grid repeatedly moves back and forth at constant speed through the whole length of the tank with frequency comparable to or less than N. In (*c*) the grid moves rapidly over a distance shorter than the tank length and stops, leaving a collapsing region of turbulence. Internal shear waves propagate ahead of the intrusive layers in (*a*) and (*c*).

1.2. *Grid mixing*

Relevant laboratory experiments of the three types are summarized in table 1. The grids vary from a single vertical cylinder moving steadily from end to end of a tank

https://doi.org/10.1017/jfm.2016.121 Published online by Cambridge University Press

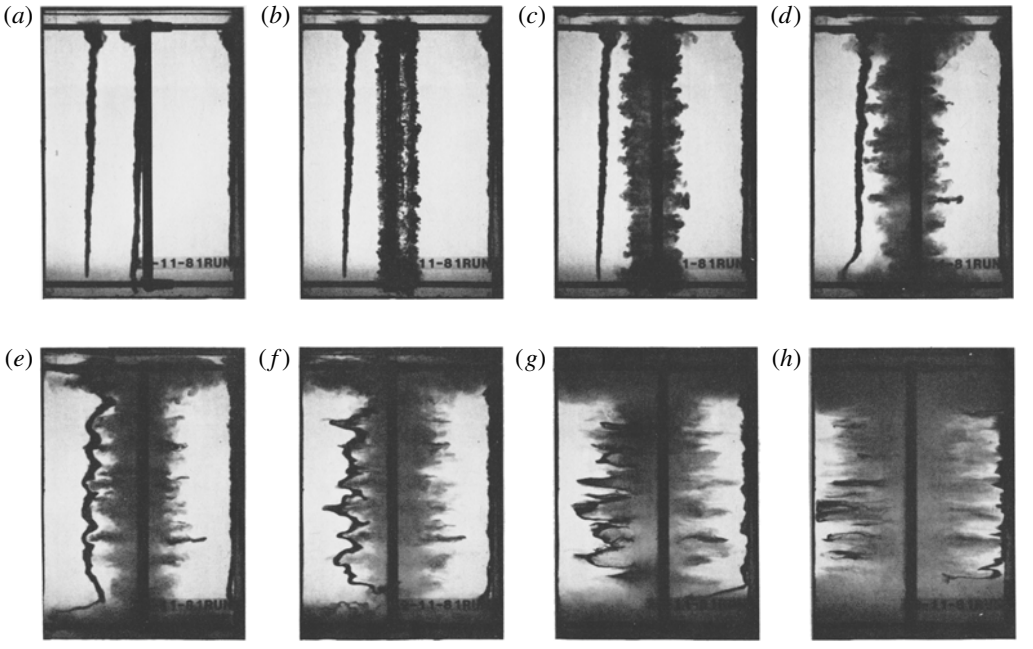


FIGURE 2. The development of horizontally spreading intrusions forming a layered structure in an experiment of type (*a*) in which a grid of vertical bars oscillates continuously in the centre of a tank filled with uniformly stratified salt solution. The grid, with solidarity parameter, $S\,(=b/M), = 0.34$, is viewed from the side. In parts (*a*) and (*b*) three columns of dye can be seen that were added before the grid motion was started at time, $t = 0$. One is close to the grid, one is on the right wall of the tank and the other half-way between the grid and the left wall. The width of the images is the tank width, 20.3 cm. The amplitude of grid motion, $a = 0.94$ cm, its frequency, $\omega = 21.3$ rad s^{-1} and the buoyancy frequency, $N = 1.98$ rad s^{-1}. The photos are at non-dimensional times, Nt, of (*a*) 0, (*b*) 0.99, (*c*) 2.77, (*d*) 6.34, (*e*) 10.7, (*f*) 22.0, (*g*) 39.8, (*h*) 113.5. The horizontal separation of the noses of the intrusions and the third column of dye is insufficient to distinguish between the vertical structures of the waves and the intrusions even at moderate values of times, Nt. (From Thorpe (1982, figure 3).)

(Park, Whitehead & Gnanadeskian 1994) to a set of parallel vertical bars that oscillates continually through a short distance along the tank (Thorpe 1982) or oscillates once at steady speed through part of the length of the tank (Maffioli *et al.* 2014). More complex grids are used, e.g. vertical bars mounted 6 cm apart along the 4 m length of the tank on strips spaced 3 cm laterally that can be oscillated longitudinally with opposite phase for alternate strips (Ruddick *et al.* 1989).

Some related experiments are not discussed here. These include Itsweire, Helland & van Atta (1986) in which a 10-layer flow passes through a stationary grid, and Britter *et al.* (1983) and Xiang *et al.* (2015) in which square-mesh grids are towed horizontally through a uniformly stratified fluid. Martin & Rehmann (2006) study the effects of the differential diffusion of heat and salt in type (*b*) experiments, but here we confine attention to experiments in which the density stratification is produced by one component, dissolved salt.

https://doi.org/10.1017/jfm.2016.121 Published online by Cambridge University Press

Fr_0	Re_0	I_0	$(Nt)_1$
Type (a) *Continuous localized mixing at end or centre of tank, with spreading/intruding layers*			
Browand *et al.* (1987, a grid identical to Hopfinger & Toly's, 1976)			
$(1.8–4.0) \times 10^2$	$(3.18–3.24) \times 10^3$	$(1.3–6.3) \times 10^4$	9.6 ± 2.5
Thorpe (1982, a grid of vertical bars)			
$(1.16–1.58) \times 10^1$	$(9.2–12.8) \times 10^2$	$(1.5–4.0) \times 10^1$	8 ± 2
Ivey & Corcos (1982, horizontal square groves cut into a vertically oscillating plate)			
$(1.88–3.6) \times 10^1$	$(1.6–3.2) \times 10^3$	$(7.1–52) \times 10^1$	Layers are 'rapidly developing'
Type (b) *Continuous mixing throughout tank*			
Ruddick *et al.* (1989, figures 2*b* and 4*c*); experiments in which layers are observed:			
$(7.6–8.6) \times 10^{-1}$	$(1.1–1.2) \times 10^2$	$(0.8–1.1) \times 10^{-2}$	>3000
Ruddick *et al.* (1989, figures 2*f* and 3*d*); experiments in which layers are not observed:			
2.4	3.32×10^2	0.24	—
Park *et al.* (1994, figure 8), typical experiment where stirring produces layers:			
0.68	5.48×10^2	0.032	>8000
Park *et al.* (1994, figure 3); typical experiment where stirring does not produce layers:			
1.82	9.50×10^2	0.39	—
Holford & Linden (1999*a*, figure 6); typical experiment where stirring produces layers:			
2.0	1.1×10^3	0.54	~ 2000
Holford & Linden (1999*a*, figure 1); typical experiment where layers are not produced:			
4.6	2.4×10^3	6.6	—
Type (c) *Short-term mixing in part of tank with collapsing turbulence*			
Liu *et al.* (1987; typical experiment (27)), mixing through half the tank length:			
22	3.8×10^3	2.3×10^2	2.1–30 'Start collapse at $Nt = 2.1$; complete collapse by $Nt = 30$'
Maffioli *et al.* (2014, figure 4), mixing through half the tank length:			
16.2	9.34×10^2	31	11

TABLE 1. Typical parameter values in three types of laboratory experiments in which a uniformly stratified fluid is stirred by moving grids. The initial Froude number, $Fr_0 = U/Nb$ (see (1.1)). The Reynolds number, $Re_0 = Ul/\nu$ (see (1.2)). The parameter, $I_0 = 1.25 \times 10^{-4} Re_0 Fr_0^2$ is a measure of the turbulent buoyancy Reynolds number as defined in § 1.2. $(Nt)_1$ gives the approximate non-dimensional time, Nt, at which layers are found or, in type (*a*) and (*c*) experiments, intrusive layers first appear. In most experiments grids composed of vertical bars are used to avoid generating internal waves or setting a vertical scale for the layers. Exceptions are Ivey & Corcos (1982) who use a plate with horizontal ridges and Browand *et al.* (1987) who use a square-mesh grid (in some experiments set obliquely at 45° to the horizontal but seemingly with no effect on the intrusion scales). The experiments of type (*a*) covered by the shown values are those listed in table 3. For types (*b*) and (*c*) the sources of data are given with the authors. The ratio, $S = b/M = 0.39$ in both the listed experiments of Holford & Linden (1999*a*).

https://doi.org/10.1017/jfm.2016.121 Published online by Cambridge University Press

Parameters characterising stirring by moving grids are a Froude number

$$Fr_0 = U/Nb, \tag{1.1}$$

and a Reynolds number

$$Re_0 = Ub/\nu, \tag{1.2}$$

where N is the initial constant buoyancy frequency of the fluid surrounding the stirring grid, typically (0.5–2) rad s^{-1}, b is the width or diameter of a grid bar and U is the grid speed or, for oscillating grids, $a\omega$, where a is the amplitude of the grid motion and ω is its frequency. We take the kinematic viscosity, ν, of the stratified fluid to be 1×10^{-6} m^2 s^{-1}. Holford & Linden (1999*a*) introduce a further parameter, the grid solidarity parameter $S = b/M$, where M is the separation distance between grid bars or the 'mesh size'. The integral turbulent length scale near the grid is assumed to be equal to b.

Table 1 lists comparative values of Fr_0, Re_0 and of I_0, a measure of the characteristic turbulent buoyancy Reynolds number or isotropy index, given by $I_0 = u_0^3/b\nu N^2$ or $\varepsilon/\nu N^2$, where u_0 is the r.m.s. velocity fluctuations, determined (following Maffioli *et al.* 2014) as $u_0 = 0.05U$ where U is the grid speed (or $a\omega$ where a is the grid amplitude and ω its oscillation frequency) and $\varepsilon = u_0^3/b$. The data used to derive values in table 1 are those given in or derived from tables or, when details are otherwise lacking, in the captions of figures in the respective papers. Figure 3 shows how the parameters Fr_0 and Re_0 of the various experiments vary in log space. The stability curves shown in the figure are discussed in §§ 2.2 and 4.1.

When stirring is over a limited domain or duration as in experiments of type (*a*) and (*c*), the intrusive layers are first seen to emerge at or near the outer edge of the turbulent region at a non-dimensional time, $(Nt)_1$, of approximately 10 (table 1). The times, $(Nt)_1$, compare to the non-dimensional time, 9.4 (a time equal to 1.5 times the buoyancy period, $2\pi/N$), for the collapse of large scales in a turbulent stratified flow in numerical studies by Staquet & Godeferd (1998), and the non-dimensional e-folding time of 4.3 found by Smyth, Zavialov & Moum (1997) for the collapse of turbulence following its isolation from surface forcing in the ocean. After the time, $(Nt)_1$, layers develop as intrusions spreading into the surrounding quiescent uniformly stratified region. They are preceded by horizontally propagating internal waves. The waves advance at the group velocity appropriate to small amplitude internal gravity waves (Thorpe 1982; Browand *et al.* 1987; Maffioli *et al.* 2014) and are explained as being internal shear waves or columnar modes (McEwan & Baines 1974; Baines 1995) generated by the intrusions. Eventually the waves reach the bounding end wall of the laboratory tank and are reflected, subsequently affecting the intrusions and the turbulent region near the grid. We return to these intrusions and internal waves in § 3.4. Only for values of Nt of several thousand are layers first observed in experiments of type (*b*).

1.3. *Numerical experiments*

We refer in §§ 4.2 and 6 to three recent direct high resolution numerical studies (DNS) made to simulate the collapse of turbulence in a stratified fluid and which relate to the laboratory experiments. The DNS are listed in table 2 with parameter values that may be compared with values of laboratory experiments in table 1. In each DNS experiment a turbulent flow with prescribed energy spectrum, independent of stratification, is imposed initially in a uniformly stratified fluid between horizontal

https://doi.org/10.1017/jfm.2016.121 Published online by Cambridge University Press

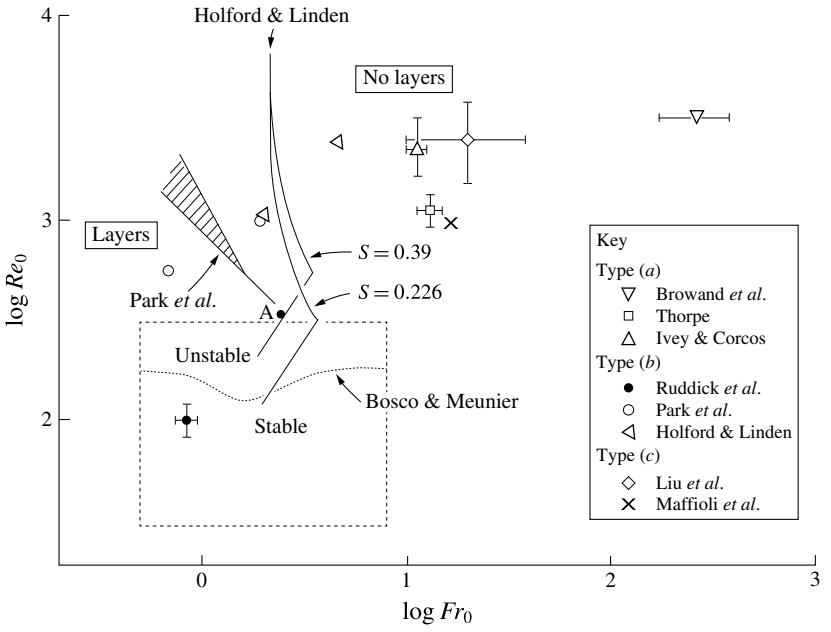


FIGURE 3. Graph of log Fr_0 versus log Re_0 for the various laboratory experiments of table 1. Layers are formed at relatively small values of Fr_0. The stability curve of Park *et al.* (1994) is shown, together with their region of marginal stability (hashed). The curve is taken from their figure 3; as noted by Holford & Linden (1999*a*) their equation for the stability boundary does not agree with the curve. Other stability curves are those derived by Holford & Linden (1999*a*) from their experiments with $S = 0.39$ (corresponding to their two points from the experiments referred to in table 1) and by Park *et al.* from experiments with $S = 0.226$, where $S = b/M$. (The conversion from Holford & Linden's values of Richardson and Reynolds numbers, Ri and Re, respectively, is $Fr_0 = [(1 - S)(\sqrt{S}Ri)]^{-1}$ and $Re_0 = Re(\sqrt{S})/(1 - S)$. The corresponding stability curve for Ruddick *et al.*'s, 1989, experiments with $S = 0.4$ is virtually the same as that shown for $S = 0.39$.) Three pairs of points from the type (*b*) experiments are marked; for these, layers are found at the lower values of log Fr_0 and no layers at the greater values of log Fr_0. No layers appear in the Ruddick *et al.*'s experiments at the point marked 'A', which lies close to both the Park *et al.* and the Holford & Linden ($S = 0.39$) stability boundaries. The stability curve for the onset of wake instability found in the lee of a steadily moving cylinder by Bosco & Meunier (2014) is marked by a dotted line. The dashed rectangle shows the parameter range of Bosco & Meunier's experiments.

upper and lower boundaries. The initial buoyancy field is taken to be one in which the density fluctuations are zero and the stratification is uniform. Turbulent mixing commences at time $t = 0$.

Diamessis & Nomura (2004) study homogeneous turbulence (with and without a mean shear but only the experiments without shear are addressed here) filling a horizontally bounded domain, i.e. a box. Their study with an equivalent Reynolds number, $Re_0 \sim 600$ (obtained from their data by using the r.m.s. turbulent velocity, $u \sim 0.05U$, following Maffioli *et al.* 2014), is aimed largely at understanding the size and three-dimensional structure of overturns in the stratified turbulent region. In their experiments with an equivalent Reynolds number, $Re_0 \sim 4000$, Venayagamoorthy & Stretch (2006) also examine homogeneous turbulence filling a box but place more

https://doi.org/10.1017/jfm.2016.121 Published online by Cambridge University Press

Authors	Exp. no.	Fr_*	Re_*	I_0
Diamessis & Nomura (2004)	RUS1	1.86	32	110
	RUS2	0.93	32	28
	RUS3	0.58	32	11
Venayagamoorthy & Stretch (2006)	—	3.2	200	900
	—	1.6	200	200
	—	0.79	200	62
	—	0.32	200	9
	—	0.16	200	2
	—	0.079	200	0.5
	—	0.032	200	0.1
Maffioli *et al.* (2014)	F0.03	0.032	485	0.5
	F0.1	0.1	371	3.7
	F0.2	0.2	371	14.8
	F1.5	1.5	371	835

TABLE 2. Numerical experiments simulating the collapse of turbulence in a stratified fluid. Here $Fr_* = u_0/Nl$ and $Re_* = u_0 l/\nu$ and $I_0 = Re_* Fr_*^2$ (or $I_0 \sim \varepsilon/\nu N^2$ evaluated at time $t = 0$ for Venayagamoorthy & Stretch's figure 6), where u_0 is the r.m.s. velocity fluctuation of the initial flow, l is the integral length scale, ν is the kinematic viscosity and ε is the initial rate of dissipation of turbulent kinetic energy per unit mass. For comparison with table 1, $Fr_0 \approx 20 Fr_*$ and $Re_0 \approx 20 Re_*$, assuming $u_0 = 0.05U$ following Maffioli *et al.* Venayagamoorthy & Stretch's experiments are not numbered.

attention on the generation of internal waves and on vortices formed at $Nt \sim 4\pi - 150$. Both Diamessis & Nomura and Venayagamoothy & Stretch provide estimates of the times of collapse of stratified turbulence that are useful later (in § 4.2) in the interpretation of type (*b*) experiments. Maffioli *et al.* (2014) study turbulence imposed initially in a rectangular region of horizontal extent smaller than the box length. The equivalent Reynolds number, Re_0, is approximately 8000. A turbulent cloud is produced that spreads laterally in a way similar that of turbulence produced by the short duration oscillation of a grid in the centre of a tank in the type (*c*) laboratory experiment described in the same paper.

1.4. *The arrangement of this paper*

Possible causes of layers in the stratified turbulent flows produced by grid mixing are discussed in § 2. These include zigzag instability and the Phillips (1972) and Posmentier (1977) instability (hereafter referred to as PPI). As explained in § 2.2, the field of motion in the wake of a horizontally moving grid bar is generally not homogeneous but structured, and the structure may affect the development of layers. Laboratory experiments of type (*a*) are described in § 3 with the main conclusions summarized in § 3.5. Type (*b*) experiments are addressed and compared in § 4 and an explanation for the height of layers in these experiments is proposed in § 4.4. A similarity of the intrusive layer heights in the type (*a*) and (*c*) experiments is found in § 5. The main conclusions are summarized and discussed in § 6.

2. Causes of layers

Any process that produces spatially periodic mixing in the vertical z-direction in a uniformly stratified fluid will generate perturbations in the density field, resulting in

https://doi.org/10.1017/jfm.2016.121 Published online by Cambridge University Press

a layered density profile with z-periodic density gradients. In an extreme case, when processes result in very efficient mixing in the layers, the density profile will exhibit layers of uniform density separated by relatively thin, highly stratified layers. Here we consider some processes resulting from instability that may lead to such spatially periodic vertical mixing and thus multiple layers in grid mixing experiments.

A set of vertical bars moving through a stratified fluid will, in its wake, shed vortices with vertical axes. Yim & Billant (2015) identify and provide references to four mechanisms that may result in the instability of a single vertical vortex in a uniformly stratified fluid: shear and centrifugal instability, radiative instability (notably associated with the spontaneous radiation of internal gravity waves and observed in laboratory experiments by Riedinger, Le Dizès & Meunier (2011)) and Gent–McWilliams instability. The type of instability that may develop depends on the radial variation of vertical vorticity in the vortex. Instability may eventually lead to the formation of layers. However a moving grid will produce multiple vortices, and it is more relevant here to consider instability of more than one vortex, either through zigzag instability or the interaction of vortices in the wake of a vertical bar.

2.1. *Zigzag instability of vortex pairs*

Billant & Chomaz (2000) and Otheguy, Chomaz & Billant (2006) describe the 'zigzag instability' of a vertical cylindrical counter-rotating vortex pair with vertical vorticity, similar to a Lamb–Chaplygin dipole, in a uniformly stratified fluid. The dipole becomes unstable to a three-dimensional instability, periodic in the vertical direction, that ultimately leads to layers. The nonlinear evolution of the instability of the vortex pair, involving Kelvin–Helmholtz and gravitational instabilities, has been investigated numerically by Deloncle, Billant & Chomaz (2008), Waite & Smolarkiewicz (2008) and Augier and Billant (2011).

Although small-scale layers are apparent close to a vertical grid bar in the startup stages of some grid-mixing experiments (e.g. Thorpe 1982, figure 8*a*), possibly generated by the instability of transient recirculating eddies (§ 2.2), it is not however evident how close-knit vertically coherent pairs of vortices might be produced by moving grids; streets of individual vortices are more likely, at least in type (*b*) experiments.

2.2. *Zigzag instability in wakes*

The wake of a vertical cylinder steadily moving horizontally through a uniformly stratified fluid when $40 < Re_0 < 200$ and $0.3 < Fr_0 < 200$ is described in experiments and a numerical model by Meunier (2012). (Values of U and b in the definitions of Re_0 in (1.1) and Fr_0 in (1.2) are taken as the cylinder speed and diameter, respectively.) Until the onset of motions in directions parallel to the cylinder axis at $Re_0 \sim 190$, the wakes in unstratified and stratified fluids are similar. At small Re_0 wakes are steady; shear layers detach from the boundary layers on each side of the cylinder, producing a pair of recirculating eddies in the wake. When $45 < Re_0 \gtrsim 180$, an array of vortices is produced in the cylinder's wake, the well-known Kármán vortex street of an unstratified fluid. The vortex array consists of two rows of vortices approximately $2b$ apart and with vortices of one row staggered in relation to those of the other. The Strouhal number (equal to b divided by the horizontal separation, B, of vortices in a row) is approximately $0.019Re_0^{1/2}$. Holford & Linden (1999*b*) describe the wakes of square vertical bars moving horizontally through a uniformly stratified fluid when $1 < Fr_0 < 1.83$. The staggered double row of vortices observed in the

https://doi.org/10.1017/jfm.2016.121 Published online by Cambridge University Press

wake of a cylinder appears for $40 < Re_0 < 180$ but, as Re_0 increases, slowly develops perturbations away from the vertical. Vertical motion develops at higher Re_0, wakes becoming more fully turbulent at $Re_0 \sim 700$. Holford & Linden (1999*a*) show that even when $Re_0 = 1030$ vertical vortices can be identified in the wake.

Although 'zigzag instability' was first used to describe the instability of single vertical vortex pairs in stratified fluids, Deloncle, Billant & Chomaz (2011) adopt the term to describe the instability of steady vortex arrays in uniformly stratified fluids, including the vortex street shed by a horizontally moving vertical bar. Deloncle *et al.* examine the stability of a vortex sheet but not how it is generated by a moving grid. For a horizontal Froude number, $Fr_h \equiv |\Gamma|/(2\pi R^2 N) \leqslant 1$, where Γ is the circulation of the vortices of radius R, and when the street spacing ratio, κ, equal to the distance between the vortex rows divided by B, is less than 0.41, they show that the vortex street is most unstable to a three-dimensional instability of the zigzag type that vertically bends the vortices. (As Deloncle *et al.* remark, the spacing ratio, κ, of vortex sheets behind two-dimensional buff bodies is usually less than 0.41.) Numerical and theoretical calculations are made with Reynolds number, $|\Gamma|/(2\pi\nu)$, equal to 5×10^4 (corresponding to an effectively inviscid flow). The vertical wavelengths, λ_z, of the fastest growing disturbance in a Kármán vortex street can be derived from Deloncle *et al.*'s figures 6 and 10. Their non-dimensional measures, $BFr_h(2\pi/\lambda_z) = 8.5$ and 5.2 when $\kappa = 0.2$ and 0.4, respectively, and $Fr_h = 0.1$, have corresponding $\lambda_z/b = 0.37$ and 0.60, respectively, supposing that (as commonly found) $B \approx 5b$, where b is the width of the vertical bar forming the vortex street. Larger values, $\lambda_z/b = 4.9$ and 8.8, are found when $\kappa = 0.2$, and $Fr_h = 1$ and 1.2, respectively.

The estimates of λ_z do not appear to have been verified experimentally or related to the thickness of layers observed in grid mixing experiments. Bosco & Meunier (2014) combine laboratory and numerical experiments to show that instability, and consequent layers, with a vertical wavelength of approximately $(4 \pm 1)b$ occurs in the wake of a steadily moving vertical cylinder of diameter b when $1.0 < Fr_0 < 5.2$ and $180 < Re_0 < 190$ (a range much lower than that at which Deloncle *et al.* estimate λ_z). The instability is similar to the classical mode A instability in the unstratified case described by Williamson (1996). Bosco & Meunier attempted to visualize the zigzag instability but it was not observed, possibly because of the limited dimensions of their laboratory tank. Turning for comparison, to the type (*b*) experiments: when $Fr_0 = 1.77$ and $Re_0 = 210$, Park *et al.* (1994, run number 2) find layers of height $h \approx 5.11b$ when a single cylindrical bar moves repeatedly back and forth along the length of a tank. This estimate of h is slightly above Bosco & Meunier's range of λ_z. (Park *et al.*'s other experiments are at greater Re_0, beyond that of Bosco & Meunier.) In two experiments by Holford & Linden (1999*a*) in which a single vertical 2.8 cm square bar moves repeatedly at constant speed through the length of a tank layers are generated with height, $h \approx 3.6b$. In these experiments $Re_0 = 746$ and 1380 (higher than the range examined by Bosco & Meunier) and $Fr_0 = 1.2$. Although this value of h is within Bosco & Meunier's range of vertical wavelengths, another experiment by Holford & Linden with a single square bar has the smaller height, $h \approx 2.3b$ when $Re_0 = 930$, $Fr_0 = 0.98$.

In summary, because of the differing ranges of Re_0, there is at best only weak evidence that the onset of zigzag instability quantified numerically by Deloncle *et al.* relates to that found experimentally either by Bosco & Meunier in the wake of steadily moving cylindrical bars, or to layers in the type (*b*) experiments with a single cylindrical bar by Park *et al.* or a square bar by Holford & Linden; it has not been established that the instability may be important in the generation of the layers produced by grid mixing. More experiments are needed to quantify the parameter ranges in which zigzag instability occurs and its scale and development.

https://doi.org/10.1017/jfm.2016.121 Published online by Cambridge University Press

Authors/experiment	a (cm)	ω (rad s^{-1})	N (rad s^{-1})	y (cm)	M/η
Browand *et al.* (1987); $M = 5$ cm, $b = 1$ cm, $s = 4$–5 cm (grid of square bars identical to that used by Hopfinger & Toly (1976)); $C = 0.29$, $\beta = 0.26$					
Figure 4	2.25	13.0	0.18	23.3	0.16
Figure 12	2.25	12.2	0.64	12.0	0.31
Figure 15	2.25	12.7	0.80	10.9	0.34
Thorpe (1982); $M = 1.91$ cm, $b = 0.64$ cm, $s = 0.56$–1.88 cm (vertical square bars); $C = 0.204$, $\beta = 0.37$					
Figure 3 (shown here as figure 1)	0.94	21.3	1.98	3.68	0.55
Figure 4	0.59	24.7	1.98	2.80	0.73
Ivey & Corcos (1982); $M = 2.54$ cm, $b = 1.27$ cm, $s = 0.92$–2.0 cm (a vertical vertically oscillating plate with horizontal grooves); $C = 0.267$, $\beta = 0.247$					
Experiment 1	1.0	25.1	0.548	8.54	0.23
Experiment 2	1.0	25.2	0.592	8.23	0.24
Experiment 26	0.48	27.9	0.387	6.18	0.31
Experiment 27	0.50	25.3	0.529	5.19	0.37

TABLE 3. Experiments of type (a) with a continuously oscillating grid in a uniformly stratified fluid. The parameters are $M =$ mesh size, $b =$ grid bar diameter/width, $s =$ stroke (as used in appendix A), and C and β are non-dimensional constants defined in (3.1) and (3.2). The values of a, ω, N, y (3.4) and M/η (with η given by (3.5)) are those available in figures or tables in the three publications.

2.3. *The Phillips/Posmentier instability*

This instability does not depend on 'structured turbulence', e.g. the presence of vortices in the wake of a grid, and nor does the PPI theory provide a prediction of a vertical scale of layers that it causes. A necessary condition for the occurrence of the PPI mechanism is that the vertical density flux generated by turbulence in a stratified fluid decreases as the modulus of the (negative) upward-vertical density gradient increases, a trend physically consistent with vertical motion being inhibited by increasing stratification or larger $|\mathrm{d}\rho/\mathrm{d}z|$. An equivalent condition addressed by Holford & Linden (1999*a*) is that the mixing efficiency, defined as the ratio of the change in the mean potential energy of the turbulent fluid to the change in available (potential and kinetic) energy, decreases as the overall (or 'bulk') Richardson number increases.

Layers observed in type (b) experiments (table 1 and figure 3) have sometimes been ascribed to PPI without evidence that the condition necessary for PPI is satisfied in the turbulent conditions of the experiments before layers form. Holford & Linden (1999*a*), however, make careful measurements of the buoyancy flux and find that, even when layers subsequently develop, in the initial state the flux increases with density gradient; layers are therefore not initiated by the PPI mechanism. (An anonymous referee suggests that PPI is not detected in the initial evolution of layers because experiments have not, so far, had sufficient resolution to accurately resolve the fluxes in the initial smooth density profile.) A further important conclusion of Holford & Linden is that the flux condition necessary for the PPI mechanism is satisfied in stratified regions once the layers are formed; a layered structure is reinforced by the mechanism (see § 3.3.2). Martin & Rehmann (2006) reach the same conclusion.

https://doi.org/10.1017/jfm.2016.121 Published online by Cambridge University Press

2.4. *Other mechanisms*

There are other mechanisms, described in later sections, by which layers may be generated. Intrusions caused by the collapse of overturns in the turbulent region generated by an oscillating grid (in type (*a*) and (*c*) experiments) are discussed in §§ 3.3.1 and 3.4. Two mechanisms in type (*b*) experiments are further possible candidates: the distortion of vertical vortices by internal waves (§ 4.4) and mixing from the upper and lower boundaries (§ 4.5).

3. Experiments of type (*a*)

3.1. *Local scales of turbulent motion*

Three examples of the oscillating grid experiments of type (*a*) are listed in table 3. In the region close to an oscillating grid where, in comparison with the effects of stratification, mechanically driven turbulence is strong, motion will approximate to the unstratified turbulence generated by biplanar grids with square bars of width, b, investigated by Hopfinger & Toly (1976). They derive empirical expressions for the r.m.s. vertical velocity fluctuations, w, and the integral length scale, l:

$$w = 2^{1/2} C(a\omega)(aM)^{1/2}/(\pi x), \tag{3.1}$$

and

$$l = \beta x, \tag{3.2}$$

at a horizontal distance, x, from the central grid position, where a is the amplitude of the grid motion, M is the grid mesh length -5 or 10 cm in Hopfinger & Toly's experiments – and ω is the grid frequency (rad s^{-1}). Values of the non-dimensional coefficients, C and β, are discussed in appendix A. The eddy time scale, l/w, increases as x^2. At some distance x, grid-generated eddies will suffer significant collapse as a result of stratification when the eddy time scale, l/w becomes comparable to the buoyancy time scale, N^{-1}, i.e. when the mean local Froude number, $Fr = w/(Nl)$, reaches a critical value. Using (3.1) and (3.2), Fr can be written

$$Fr = 2^{1/2} Cy^2/(\pi \beta x^2), \tag{3.3}$$

where

$$y = (aM)^{1/4}(a\omega/N)^{1/2} \tag{3.4}$$

is a length scale determined by the grid size and motion, and by the initial uniform buoyancy frequency, N.

All the experiments of type (*a*) listed in table 3 find that η, the distance of the edge of the turbulent region from the mid-position of the oscillating grid, and the thickness, h, of intrusions measured at the edge of the turbulent region, are linearly proportional to y, i.e.

$$\eta = \alpha y \tag{3.5}$$

and

$$h = \gamma y, \tag{3.6}$$

where α and γ are non-dimensional coefficients that vary from one set of experiments to another. (The thickness of intrusive layers is approximately equal to the distance between neighbouring intrusions and, where several adjoining intrusions can be identified in experiments, is conveniently, easily and commonly estimated as the

https://doi.org/10.1017/jfm.2016.121 Published online by Cambridge University Press

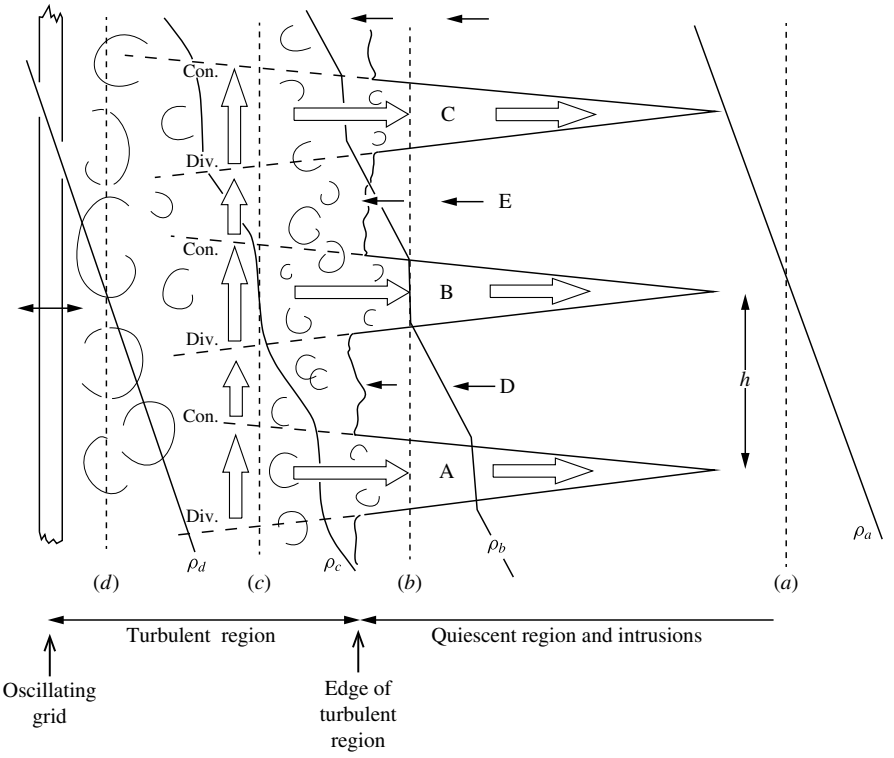


FIGURE 4. Notional sketch of the production and maintenance of intruding layers in type (*a*) experiments. In this vertical section, the oscillating grid is at the left and the quiescent uniformly stratified fluid to the right. Three layers emerging from the turbulent region and intruding into the quiescent fluid are drawn, A, B and C, with return flows, D and E, between A and B and between B and C, respectively. Vertical profiles of mean density are shown in the quiescent region at (*a*), near the edge of the turbulent region at (*b*), within the turbulent region at (*c*) and close to the oscillating grid at (*d*), and labelled ρ_a–ρ_d, respectively. The averaged scale, h, is that commonly used to represent layer height. It may, as sketched, exceed that thickness of the regions of constant density in the intrusions emerging at the edge of the turbulent region. The length of vertical arrows at (*c*) indicate how the magnitude of the mean vertical flux of buoyancy varies with the density gradient, increasing the density in regions of convergence ('con.') and decreasing density in regions of divergence ('div.'), and so tending to maintain the layers of small (negative) vertical density gradient in the regions feeding the intrusions and enhancing the gradients above and below these regions. The sketch differs notably from that of Browand *et al.* (1987, figure 11) and reproduced by Maffioli *et al.* (2014, figure 1) in that the intruding layers are shown to begin within the turbulent region, being initially formed by the collapse of large-scale overturning eddies or 'blobs' that are relatively uniform in density. The vertical collapse and horizontal spreading of the blobs is asymmetrical, favouring motion away from the grid, because of the horizontal variation in Reynolds stress across their width. Internal shear waves (not drawn and of undetermined phase in relation to the intrusions; see § 6) are found to the right of the intrusions, propagating ahead of them.

average distance between them. As sketched later in figure 4, however, this scale may exceed that of intrusions at the edge of the turbulent region.) The consistency found between the three experiments suggests that the Hopfinger & Toly scaling,

https://doi.org/10.1017/jfm.2016.121 Published online by Cambridge University Press

x/η	h/L_O	Fr
0.39	1	1.85
0.53	1.85	1
1	6.58	0.28

TABLE 4. Values obtained from Browand *et al.*'s (1987) type (*a*) experiments using $C = 0.29$, $\beta = 0.26$, $\alpha = 1.34$, $\gamma = 0.34$ and listed in order of increasing x/η through the turbulent region. ($x/\eta = 1$ is the location of its mean boundary. h/L_O increases with x/η.)

(3.1) and (3.2), is valid for the three different grid types described in table 1, type (*a*) experiments. Browand *et al.* (1987) find values of α and γ equal to 1.34 ± 0.27 and 0.34, respectively. The respective values are 0.94 and 0.34 in Thorpe's (1982) experiments, and 1.34 and 0.32 in Ivey & Corcos's (1982) (see Thorpe 1982). Browand *et al.* use a vertical horizontally oscillating grid with mesh and bar size identical to one used by Hopfinger & Toly. Extrapolating from Hopfinger & Toly's results, they adopt the values $C = 0.29$ and $\beta = 0.26$. From (3.3) and (3.5), the Froude number at the edge of the turbulent region, $x = \eta$, can be estimated: $Fr = 0.28$. This is consistent with the observation by Dickey & Mellor (1980) that the character of motion in the wake of a horizontal grid moving vertically upwards in a uniformly stratified fluid changes from turbulence to internal waves where $Fr = 0.27$. Using (3.2), (3.5) and (3.6), at the boundary of the turbulent region, $h/l = \gamma/\beta\alpha = 1.01 \pm 0.20$, or $h \approx l$ at $x = \eta$ as speculated by Thorpe (1982). Values of C and β are unknown for the grids used by Thorpe and Ivey & Corcos but can be inferred as $C = 0.204$, 0.267 and $\beta = 0.37$, 0.247, respectively by making the similarity assumption that $Fr = 0.28$ and $h = l$ at $x = \eta$.

The local Ozmidov length scale, $L_O = \varepsilon^{1/2}/N^{3/2}$, equals

$$L_O = 2^{3/4} C^{3/2} y^3 / (\pi^{3/2} x^2 \beta^{1/2}), \tag{3.7}$$

taking the rate of dissipation of turbulent kinetic energy per unit mass, ε, as w^3/l. Using (3.3)–(3.6), corresponding values of x/η, h/L_O and Fr from Browand *et al.*'s experiments are found and specified in table 4. The ratio h/L_O exceeds 1 at $Fr = 1$ and, as shown by (3.3), Fr decreases as x/η increases through the turbulent region. At the edge of the turbulent region, h (and therefore l), is much greater than the scale of the largest overturning eddies, L_O, so that the turbulent motion is largely horizontal.

As conjectured by Maffioli *et al.* (2014) the local Froude number, Fr, provides values that determine the character of the turbulent flow. Further evidence that a Froude number characterises the state of the stratified turbulent motion is provided by the stability curves in figure 3: layers form only when Fr_0 is less than a value of approximately unity. As outlined in appendix B, the local buoyancy Reynolds number, I, does not provide such a similarity parameter. Moreover, the local Reynolds number, $Re = wl/\nu$, is independent of x and therefore also cannot be an effective parameter to define the local state of turbulence.

In summary, the size, h, of layers in the type (*a*) experiments is given by $h = \gamma y$, with $\gamma = 0.33 \pm 0.01$. The bar scales of the three experiments listed in table 1, $b = 1.0$ cm, 0.64 cm and 1.27 cm, respectively, do not appear to provide the size or scaling of the layer thickness, h, that might be expected if the layers result from zigzag instability of a vortex street (e.g. $h \approx 4b$; § 2.2). Indeed how the instability of a vortex pair or vortex street might apply to the disorganized mêlée of vortices shed by a rapidly oscillating grid is not obvious.

https://doi.org/10.1017/jfm.2016.121 Published online by Cambridge University Press

3.2. *The origin of layers*

3.2.1. *Collapsing overturns*

Browand *et al.* (1987) note that although intrusive layers are not visible until they reach the edge of the near-grid turbulent region, the turbulence itself is affected by the layering at times of (2–3)Nt, before the intrusions emerge and become apparent at $Nt = 9.6 \pm 2.5$ (table 1). They also remark that 'an effective origin in time' for the advance of intrusive layers is 'much nearer to the onset of grid motion' than to some other, more arbitrary, initial time. Similarly, Thorpe (1982) finds that the horizontal extent of layers is proportional to $y(Nt)^p$, where t is the time elapsed from the start of grid oscillation and p is a constant near 0.4; layers appear to be first formed near the oscillating grid and at a time close to that at which grid stirring begins.

We shall suppose that initially 'blob-like' roughly spherical overturns with height of order L_O are produced within the turbulent region, and that the blobs collapse and spread to supply fluid that initially forms the intrusions. Whilst noting the uncertainty in characterising the intrusion height by the measured scale, h, and an overturn by L_O, if volume is (approximately) conserved the height of an overturn leading to an intrusion must equal or exceed that of the intrusion unless the fluid of the overturn is supplemented during its collapse.

3.2.2. *The size of overturns*

It is evident from table 4 that only close to the grid, at $x/\eta < 0.39$, does the Ozmodov scale, L_O, exceed h. There are reports, however, of layers of thickness exceeding L_O in laboratory experiments. Browand *et al.* (1987) noticed layers with a vertical scale 'approximately 7 times the estimated Ozmidov scale at $Nt = 10$', the time, t, being that when the front of the turbulent region surrounding the grid begins to break up with the formation of layers. This estimate is in accord with the value h/L_O at $x/\eta = 1$ in table 4. In experiments of type (b) with continuous stirring throughout the tank, Ruddick *et al.* (1989) find that 'the observed layer thicknesses were always larger than the Ozmidov scale'. They estimate L_O as $(5K_\rho N^{-1})^{1/2}$ where K_ρ is the molecular diffusivity of density (rather than an eddy diffusivity that might be more appropriate). This gives $L_O = (0.2\text{–}0.3)$ mm or less, smaller than the layers which are typically 2 cm in height. The smallest layers observed are of scale 0.6 cm after 150 min of grid stirring. In one experiment they do however report: 'irregular variations in the density gradient of scale 1–2 cm were apparent. . . . together with finer-scale striations of approximately 1 mm spacing'. The greater-than-L_O thickness of layers may be because of layer merging leading, in the long-duration experiments of type (b), to thicker layers. Indeed Ruddick *et al.* comment that, in one experiment, 'the thicker layers may have formed by the merging of thinner layers'. Although recognised as a potentially significant process by Browand *et al.* (1987), Liu *et al.* (1987), Balmforth, Llewellyn Smith & Young (1998) and Wunsch & Kerstein (2001), there appears to be insufficient quantitative information to determine the general importance of layer merging in establishing the height of intrusions. All the type (b) experiments show that layers can exist and survive within a turbulent, actively stirred region through which a grid is moving.

An r.m.s. displacement (or Thorpe) scale, L_T, is often used to characterise the vertical scale of density overturns. From observations in a freshwater lake and at sea Dillon (1982) suggests $L_O/L_T \sim 0.8$ while Peters, Gregg & Toole (1988) and Ferron *et al.* (1998) conclude $L_O/L_T \sim 0.95$; both relations imply that the r.m.s. displacement scale, L_T, exceeds L_O. In numerical experiments on collapsing stratified turbulence, however, Mater, Schaad & Venayagamoorthy (2013) find the ratio, L_T/L_O,

https://doi.org/10.1017/jfm.2016.121 Published online by Cambridge University Press

increases as the characteristic Froude number, Fr, decreases, with $L_T \sim L_O$ where $Fr = 1$. If the numerical results can be used as a guide, they imply that $L_T > L_O$ in the outer part of the turbulent region surrounding the oscillating grid. The scale L_T is, however, observed to be distributed log normally (Stansfield, Garrett & Dewey 2001) with some individual values much greater than the mean. Itsweire (1984) finds that the maximum size of overturns, L_{max}, is 2.74 times the r.m.s., L_T, a scaling supported by measurements in grid-generated turbulence by De Silva & Fernando (1998). Taking $L_T = (1/0.8)L_O$ in accord with Dillon's results, and $L_{max} = 2.74L_T$, gives $L_{max} \approx 3.4L_O$. Since (from (3.7)) $L_O \propto x^{-2}$ and $L_O/h = 1$ at $x/\eta = 0.39$ (table 4), $L_{max}/h \approx 3.4$ at $x/\eta = 0.39$ and $L_{max}/h \approx 1$ at $x/\eta = 0.72$. It follows that within the turbulent region near $x/\eta \sim 0.4$, overturns occur of height, L_{max}, substantially exceeding h.

Similar layers can be seen at the same vertical location on the two sides of the grid oscillating in mid-tank shown in figure 2(*d–g*). This implies that layers have a common origin near the grid and, at least for the grid in the figure with solidarity parameter, $S = 0.34$, a structure that survives the stirring motion of the grid (as in the type (*b*) experiments) by transmitting information through it, perhaps initially by fluid transfer but more likely, in later stages, by pressure gradients.

3.3. *Sustaining layers within the turbulent region*

3.3.1. *Spread of large overturns*

Apart from the conclusions reached in § 3.2, there is little information provided by the laboratory experiments about the processes within the turbulent region that lead to the generation and maintenance of intrusions. The intruding fluid moving from the turbulent region must be replaced by ambient fluid in a return flow into the turbulent zone as sketched in figure 4 or, for example, in Browand *et al.*'s (1987) figure 11. Figure 4 shows three intruding layers, A, B and C. Density profiles are shown at four horizontal locations, (*a–d*). The vertical density gradient in the return flows, D and E, between intrusions, is modified as the return flow narrows as it approaches and enters the turbulent region, tending to strengthen the density gradients above and below the spreading fluid and inducing within the turbulent region a variation in the vertical density gradient. Browand *et al.* imagine a process of self-regulation in which, if an intrusion slows down, so does the return flow. Consequently the grid, deprived of this stratified return flow, is able to mix the fluid more thoroughly, supplying the intrusion with more well-mixed fluid, resulting in an increase in its speed. The converse applies: if an intrusion speeds up, so does the return flow resulting in a less well-mixed supply and a subsequent decrease in the speed of the intrusion. This control process does not however lead to an estimate for h.

A further feature in the spreading of relatively mixed layers within the turbulent layer is the horizontal variation of Reynolds stress, $\langle \rho uw \rangle$. Layers span a region of rapidly decreasing Reynolds stress ($\langle \rho uw \rangle \propto x^{-2}$ through (3.1) since the fluctuations in the vertical and horizontal velocity fluctuations, w and u, are of similar magnitude near the grid). The eddy stresses on the grid side of a relatively well-mixed blob will impede its collapse under gravity (driven by the horizontal pressure gradients resulting from the differences in density within and outside the blob) more than do the stresses of smaller weaker eddies on the side of a blob furthest from the grid. A spread of a blob away from the grid is therefore favoured, and this must help induce the return flow.

https://doi.org/10.1017/jfm.2016.121 Published online by Cambridge University Press

3.3.2. *A Phillips/Posmentier process*

Although PPI does not appear to initiate layers (§ 2.3), the instability mechanism may help sustain layers once they are formed (Holford & Linden 1999*a*). Assuming that Holford & Linden's finding that PPI can occur in turbulent but layered conditions and that those in their type (*b*) experiments are similar to those near the oscillating grid in the type (*a*) experiments, the turbulent flux of density will decrease as the negative vertical density gradient increases. There is therefore a decrease in the upward-vertical buoyancy flux where the negative density gradient is large, i.e. within the layers above and below the intrusion at section (*c*) in figure 4, and an increase in the upward buoyancy flux where the negative density gradient is small, i.e. within the fluid of the intrusion. These variations in flux are indicated by the vertical arrows in figure 4. Just as in Phillips' instability theory the result is that the density near the base of the intrusion is decreased and that near the top is increased; differences in density across the layers above and below the intrusion are increased. The region of relatively mixed fluid originally in an overturn is enhanced and sustained within the turbulent region, and so too are the pressure gradients that lead to its spreading.

3.4. *The speed of intrusions and internal waves*

3.4.1. *Internal shear waves*

The greatest speed at which internal waves generated by the grid turbulence can radiate horizontally corresponds to that of internal shear waves or columnar modes and is given by the horizontal component of the group velocity, $c_{gx} = N/m$, where m is their vertical wavenumber (putting $k = 0$ in (C 2) in appendix C). Vertical dye lines in the stratified ambient water ahead of the intrusions in the experiments by Thorpe (1982) and Browand *et al.* (1987) show the early arrival of oscillations with vertical wavelengths, $\lambda_z\,(= 2\pi/m)$, roughly twice the vertical distance between the intrusions at a time consistent with the propagation speed c_{gx}. There are two shear layers produced by the shear waves, one of positive horizontal vorticity and one negative, in each internal wave vertical wavelength, a point to which we return in §§ 4.4 and 6. Maffioli *et al.* (2014, and private communication with Dr A. Maffioli, October '14) find that the vertical wavelength of the horizontally travelling internal waves, judged from twice the distance between pearlessence-revealed shear layers in their laboratory experiments, is approximately twice that of the intrusions. This is consistent with the findings of Browand *et al.* and Thorpe. In § 3.4.4 we address the question of why a scale of approximately $2h$ is favoured.

3.4.2. *The speed of waves and intrusions in other studies*

The speed at which internal waves and intrusions spread in a uniformly stratified fluid of buoyancy frequency, N, is discussed by Bolster, Hang & Linden (2008) and by Maurier & Linden (2014). In their 'lock-break' laboratory and numerical experiments the latter show that intrusions spread at uniform speeds after a short initial stage of acceleration and until intrusions are affected by the reflection of internal waves from the end of the tank. An 'intermediate intrusion' of fluid with density equal to the mean of those at the upper and lower horizontal boundaries spreads at half-tank depth with a speed of approximately half that of density currents spreading along the upper or lower boundaries. These boundary density currents are found by Maxworthy *et al.* (2002) and by Bolster *et al.* to advance at speeds of approximately $0.25NH$, where H is the tank depth. Maurier & Linden show that the speed of intermediate intrusions is explained by noting that they are equivalent to two boundary density currents, one

https://doi.org/10.1017/jfm.2016.121 Published online by Cambridge University Press

above a surface dividing the intrusion into two at the half depth, the other below. Since each of these is in an effective depth of $H/2$, their speeds are $0.25N(H/2) = 0.125NH$.

Gravity currents with density greater or less than that in the ambient uniformly stratified fluid, namely those spreading along the lower or upper boundaries, respectively, generate internal waves. Long internal shear waves of mode 1 advance ahead of them; the long-wave group velocity $c_g = NH/\pi$ exceeds the gravity current speed, $0.25NH$. The speed of long mode 2 internal shear waves, $NH/2\pi$, is, however, less than that of these density currents and so mode 2 waves cannot propagate ahead of them. Similarly intrusions of intermediate density spreading into uniformly stratified fluid at height less than $0.27H$ or greater than $0.73H$ above the bottom travel at speeds less than the mode 1 internal waves but greater than the second mode waves (Bolster *et al.* 2008). However, intrusions spreading at heights between $0.27H$ and $0.73H$, for example those with the mean density, which travel at mid-depth, produce long mode 2 waves (by symmetry) that advance at speed $NH/2\pi$. These are in excess of the speed of the intrusion and are able to propagate ahead of it.

3.4.3. *Boundary density currents generated by grid mixing*

Because there is no vertical density flux through the horizontal boundaries at the top and bottom of the tank, mixing by the grid forms layers of relatively uniform density, that at the upper boundary being of density slightly greater than that in the ambient fluid at the top of the tank. Similarly the mixed layer at the lower boundary is slightly less dense than that in the ambient at the bottom. These layers intrude horizontally as density currents into the ambient fluid close to the respective horizontal boundaries (e.g. as is visible near the upper boundary in figure 2), and will generate long internal waves mainly of mode 1 which travel at a speed NH/π. It is shown in appendix C that these appear unlikely to affect the intrusions emerging in the experiments from the turbulent region at times, Nt, less than 16, with the possible exception of those intrusions that neighbour these boundary currents.

3.4.4. *The speed of the intrusions in the grid mixing experiments*

Thorpe (1982) and Browand *et al.* (1987) find that the mean non-dimensional speed of intrusions, $\mathrm{d}l_i/\mathrm{d}t$, is approximately given by

$$(1/Nh)\mathrm{d}l_i/\mathrm{d}t = \chi\,(Nt)^{-q}, \tag{3.8}$$

where l_i is the length of an intrusion and h is the intrusion height. In Browand *et al.*'s experiments the non-dimensional coefficient χ varies from approximately 0.49 to 1.0 as the exponent, q, varies from 0.3 to 0.5 when Nt exceeds a value of approximately 4 and before internal waves reflect from the end of the tank. In Thorpe's experiments $\chi \sim 0.69$ and $q \sim 0.56$ when $2 \leqslant Nt \leqslant 20$. These values give intrusion speeds, $\mathrm{d}l_i/\mathrm{d}t$, ranging from $0.25Nh$ to $0.32Nh$ in Browand *et al.*'s experiments and equal to $0.19Nh$ in Thorpe's, at the non-dimensional time, $(Nt)_1 \approx 10$ (table 1), when intrusions are observed to emerge from the turbulent region. (Greater speeds are observed at smaller Nt.) These speeds exceed Maurier & Linden's estimate, $0.125Nh$, of the speed of intermediate intrusions confined between levels separated in the vertical by h (§ 3.4.2). They are indicative of different forcing processes. Unlike the constant speed intrusions formed by lock-breaking and continually supplied by fluid from behind the 'lock', or sustained by mixing from the mean level of a vertically oscillating horizontal grid

https://doi.org/10.1017/jfm.2016.121 Published online by Cambridge University Press

(De Silva & Fernando 1998), the type (*a*) intrusions continually decelerate (as in (3.8)). This is consistent with their formation being transient and not sustained as in the 'lock-break' scenario.

The initial speeds of advance of intrusions from the turbulent region, ranging from $0.19Nh$ to $0.32Nh$, exceed the horizontal group velocity, $c_{gx} = N/m = Nh/2\pi \approx 0.16Nh$, of internal shear waves with vertical wavelength, h, which therefore cannot propagate ahead of the intrusions. The advance of a vertical array of intrusions separated by a vertical length, h, will however generate a spectrum of internal waves. It is shown in appendix D that only waves with vertical scale equal to or exceeding $2h$ can propagate ahead of the intrusions. This is in accordance with the observed wavelengths, $\lambda_z \sim 2h$ (§ 3.4.1). Because intrusion speeds decrease with Nt, however, waves of vertical scale h are able to advance faster than the intrusions when Nt is sufficiently large. Like the intrusions themselves, the scale of the waves dominant at large times must be related to the presently unknown spatial and temporal distribution of collapsing mixed regions within the turbulent region.

3.5. *Summary of §§ 3.1–3.4*

It is yet to be shown whether zigzag instability can generate the layers observed in the type (*a*) experiments (§ 3.1), but it appears unlikely except perhaps as a grid of vertical bars is first set into motion (§ 2.1). Holford & Linden (1999*a*) find that the PPI mechanism may help sustain, but not cause, layers in the turbulent region. The local Froude number, Fr, characterises the variation of the state of turbulence with distance from its generation by the moving grid. The height of overturns, L_{max}, well within the turbulent layer (e.g. at $x/\eta \sim 0.4$) substantially exceeds the layer height, h (§ 3.2.2). Overturns are consequently sufficiently large to produce intruding layers of the height, h, observed at the edge of the turbulent region. In § 3.2.1 it is shown that the variation in time of the intrusions' horizontal extent is consistent with their starting at about the time when the grid is first set in motion. There is a similarity of layers on the two sides of a grid oscillating in the centre of a tank (§ 3.2.2). These conclusions imply that layers in continuously forced, type (*a*) (and possibly transiently forced, type (*c*)) experiments are formed soon after the grid stirring begins and may have connection through an oscillating grid.

In § 3.4 it is found that the leading internal waves propagating ahead of the intrusions have a vertical wavelength of approximately $2h$, twice the thickness of the layers; waves of smaller vertical scale do not travel fast enough to advance more rapidly than the intrusions when they are first observed, emerging from the turbulent region. The sometimes remarkable vertical periodicity and regularity of intrusions remains unexplained.

4. Experiments of type (*b*)

4.1. *Stability curves*

Three experiments of type (*b*) in which the whole tank is stirred are listed in table 1. Layers are not observed until after stirring has continued for times exceeding some thousands of buoyancy periods. The stability curve determined empirically by Park *et al.* (1994) is shown in figure 3, together with a neighbouring (hatched) region in which they report that it is uncertain whether layers are formed or not. The stability curve separates two regimes recognised in their experiments: a regime of sufficiently low Re_0 and low Fr_0 in which layers are observed and a regime at

https://doi.org/10.1017/jfm.2016.121 Published online by Cambridge University Press

higher Re_0 and Fr_0 in which no layers appear. Parameter values of two of Park *et al.*'s experiments, one in each regime, are given in table 1 and shown as circles in figure 3. The experiments in which layers are observed by Ruddick *et al.* (1989) lie within Park *et al.*'s layer regime even though the apparatus and experimental details differ (e.g. Park *et al.* have one stirring rod, Ruddick *et al.* have many). Ruddick *et al.*'s experiment in which no layers form (point marked as 'A' in figure 3) lies very close to the (imprecise) position of the stability curve, consistent with the expectation from Park *et al.*'s study that the turbulent flows are at best weakly unstable.

As mentioned in § 2.3, Holford & Linden (1999*a*) find that PPI is not a cause of layers. Rather they conclude that vertical mixing resulting from bending of vertical vortices shed by the moving grid bars causes the layers. Their explanation does not, however, account for the height of observed layers. They establish an empirical stability curve dividing the regions in which layers are formed from that in which they are absent. The curve depends on the grid scale parameter S. Two of the curves are shown in figure 3. These correspond to the value $S = 0.39$ in Holford & Linden's experiments referred to in table 1 and shown as points in figure 3, and to $S = 0.226$ corresponding to Park *et al.*'s experiments (although there, with only one stirring bar, the mesh size, M, is uncertain. It is somewhat arbitrarily taken as the tank width. This may account for the difference between the Park *et al.*'s stability curve and Holford & Linden's curve $S = 0.226$).

4.2. *The effect of turbulence ahead of the grid*

Ambient turbulence in the tank, encountered and supplemented by the stirring grid after its first cycle, may affect the formation of vortices in the grid wake which are found by Holford & Linden to be necessary for the generation of layers. Turbulence produced by the moving grid decays in time. The repetition period of stirring by the cycling grid depends on position along the length of the tank. At the centre this period is L_s/U, where L_s is the horizontal length of grid motion, and at the ends of the grid stroke it is $2L_s/U$. The r.m.s. time period is $T_* = \sqrt{(8/3)}(L_s/U)$. (This is found by integrating and summing the squares of X and $(1 - X)$, where XL_s is the distance along the tank from the end of a grid stroke, then taking the square root.) NT_* characterises the non-dimensional mean time between grid stirring events. Suppose that the processes producing layers as the grid passes by (e.g. those to be described in § 4.4) are only effective if the turbulence left by previous cycles of the grid has decayed sufficiently. Marginal conditions for layer generation exist when the time, T_d, for turbulence to collapse is equal to T_*, i.e. when

$$NT_d = \sqrt{(8/3)}(NL_s/U), = \sqrt{(8/3)}(L_s/b)Fr_0^{-1}. \tag{4.1}$$

If the non-dimensional time for the decay of turbulence in a stratified fluid is known as a function of Re_0 this equation defines the stability boundary separating conditions in which layers can or cannot be formed. Values of NT_d smaller than $\sqrt{(8/3)}(L_s/b)Fr_0^{-1}$ imply conditions in which turbulence has decayed substantially between grid strokes so that the processes leading to layers can operate, unaffected by the residual turbulence. Alternatively, given the relation between Re_0 and Fr_0 defined by the stability curves of figure 3 and values of L_s/b in the related experiments, (4.1) can be used to determine the value of NT_d as a function of Re_0 for which marginal conditions are found.

Points at various values of Re_0 (with corresponding values of Fr_0) on the stability curves of Park *et al.* (1994) and Holford & Linden (1999*a*) shown in figure 3 are

https://doi.org/10.1017/jfm.2016.121 Published online by Cambridge University Press

Re_0	NT_d	Stability curve
370	4.5	Park *et al.* (1994)
600	6.9	Park *et al.* (1994)
1000	10.1	Park *et al.* (1994)
1020	12.8	Holford & Linden (1999*a*) $S = 0.39$
3070	15.7	Holford & Linden (1999*a*) $S = 0.39$

TABLE 5. The variation of non-dimensional turbulent decay times, NT_d, with Re_0, inferred from (4.1) and the stability curves of figure 3, in type (*b*) experiments.

selected. Table 5 gives values of the non-dimensional turbulence collapse time, NT_d, determined using (4.1) for which conditions are marginal and turbulence does not affect the process of layer formation. These values increase with Re_0. They span the times $(Nt)_1 \sim 10$ for the emergence of layers from the turbulent region in type (*a*) experiments, and those of numerical experiments mentioned in § 1.3 and listed in table 3. In the latter $Nt \sim 2\pi$ and 10 are found by Venayagamoorthy & Stretch (2006) and by Maffioli *et al.* (2014, and private communication with Dr A. Maffioli, June, 2015) to characterise the cessation of overturning and the suppression of turbulent mixing when $Re_0 \sim 4000$ and 8000, respectively. Diamessis & Nomura (2004) find $Nt = 4.5$ when the volume fraction of overturns tends to zero, when $Re_0 \sim 600$.

These times imply that in the type (*b*) experiments the production of overturning eddies by the turbulence virtually ceases between successive mixing by grids in those type (*b*) experiments listed in table 1 in which layers are formed. For example, selecting two type (*b*) experiments listed in table 1 where stirring produces layers, the time $\sqrt{(8/3)}(L_s/b)Fr_0^{-1}$ is 14.6 in Park *et al.*'s figure 8 at $Re_0 = 548$, and 16.8 in Holford & Linden's figure 6 at $Re_0 = 1100$. Both exceed values of the non-dimensional turbulent decay times, NT_d, in table 5. In these experiments, on average the grids advance into relatively weak residual turbulence left from their last cycle. Coherent vortices (§ 2.2) shed by the grid may then survive in the turbulent motion left from earlier grid stirring. In contrast, layers are not observed in conditions in which a vortex wake may be suppressed by turbulence still active from earlier grid stirring.

4.3. *The layer height*

Layer heights in type (*b*) experiments are found to be related to U/N. Park *et al.* (1994), stirring with single vertical cylindrical bars of diameter, $b = 1.29$, 2.26 and 3.37 cm, find

$$h \text{ (cm)} = 2.6U/N + 1 \text{ cm}, \tag{4.2}$$

independent of b, with h, U and N in cgs units, over a range of U/N from approximately 0.5 to 3 cm. Holford & Linden (1999*a*) use a variety of grids composed of 1–8 square vertical bars, b ranging from 0.65 to 3.15 cm. They conclude

$$h = 3.07U/N, \tag{4.3}$$

again independent of b, in the range of U/N from approximately 0.7 to 4.2 cm. (As mentioned in § 1.2, Ruddick *et al.* (1989) have a complex stirring device with cylindrical bars of diameter 1.2 cm. Given values of h (cm) are $2.72U/N$ for $U/N = 0.73$ cm and $3.27U/N$ for $U/N = 0.64$ cm, fairly close to and bracketing values in (4.3). Here U is taken as $a\omega/\sqrt{2}$ where ω is the grid frequency and a

https://doi.org/10.1017/jfm.2016.121 Published online by Cambridge University Press

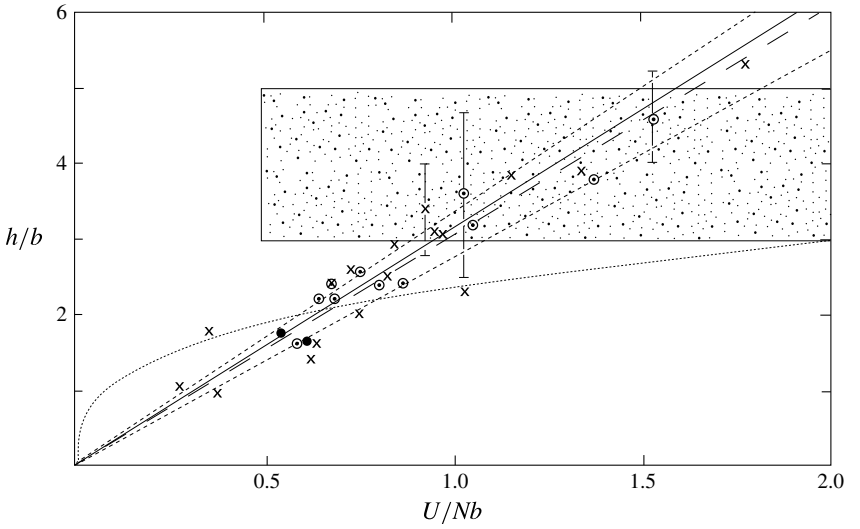


FIGURE 5. The variation of h/b with $U/Nb\,(=Fr_0)$ for type (b) experiments. Points (●) are from Ruddick *et al.* (1989), crosses (×) are from Park *et al.* (1994) and open circles (○) are from Holford & Linden (1999*a*). The fitted long dashed line is $h/b = 3.03U/Nb$, and the short dashed lines, $(3.03 \pm 0.3)U/Nb$, (4.4), indicate its possible uncertainty. The full line is the relation (4.6) derived in § 4.4 in which vortices shed by the grid bars are supposed to be bent by internal waves moving with the grid at speed U. The dotted curve is the best fit, (5.1), determined by Maffioli *et al.* (2014) from their laboratory experiments of type (c), although these are in the range $16 < U/Nb < 74$, beyond that of the type (b) experiments (see figure 6). The stippled region indicates the range of h/b observed by Bosco & Meunier (2014).

is the amplitude of the grid motion.) Figure 5 is a graph showing the variation of h/b with U/Nb for the type (b) experiments. There is general alignment of points between the lines

$$h/b = (3.03 \pm 0.3)U/Nb \tag{4.4}$$

(or $h/b = (3.03 \pm 0.3)Fr_0$).

The vertical scale of the instability in the wake of a horizontally moving vertical cylinder found by Bosco & Meunier (2014) to be $(4 \pm 1)b$, independent of Froude number, is shown by the stippled region of figure 5. It is inconsistent with the type (b) experiments. As shown in figure 3, however, Bosco & Meunier's study is at lower Reynolds number than that of the type (b) experiments. Further study is merited.

4.4. *Internal waves and vortices*

Although internal waves are not reported in the long-running experiments of type (b), it is probable that they are generated, particularly in the relatively low forcing conditions (larger NT_d) when layers are observed and the turbulence in the fluid into which the grid moves is relatively weak. Suppose that the motion of the grid through the tank at speed U generates horizontally travelling internal waves. The optimally generated waves are those with group speed, $c_{gx} = N/m$ (and, as shown in appendix C, an equal phase speed), that match (and remain in phase with) the grid: $c_{gx} = U$, where

https://doi.org/10.1017/jfm.2016.121 Published online by Cambridge University Press

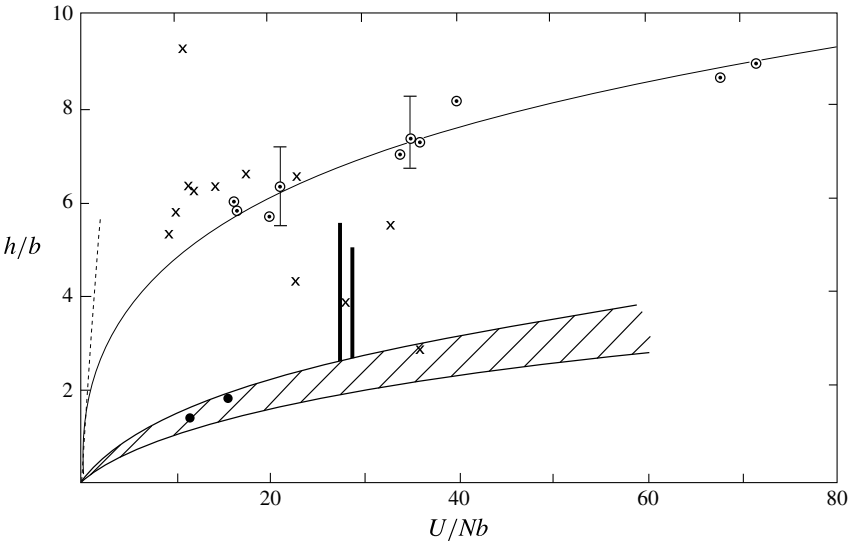


FIGURE 6. The variation of h/b with $U/Nb\,(=Fr_0)$ for (i): the type (a) experiments by Thorpe (1982) indicated by the hatched range, including the two referred to in table 3 shown by ●, and Browand *et al.* (1987), marked by bold range bars (with an off-scale point at $h/b = 8.7$, $U/Nb = 180$ omitted); (ii) the type (b) experiments (indicated by the dashed line at relatively small U/Nb and shown in greater detail in figure 5); and (iii) type (c) experiments, where the circles (○) are points from Maffioli *et al.*'s (2014) experiments fitted by the long-dashed line, (5.1), and where the vertical bars indicate uncertainty, and the crosses (×) are from the experiments by Liu *et al.* (1987) (see appendix E).

$m = 2\pi/\lambda_z$ is the vertical wavenumber and λ_z is the vertical wavelength of the waves. The latter is therefore given by

$$\lambda_z = 2\pi U/N, \tag{4.5}$$

provided that vertical wavelengths of appropriate scale are excited. Using the relation between U/Nb and h/b (4.4) of figure 5 it follows that $\lambda_z = (2.07 \pm 0.21)h$; internal shear waves that propagate with the speed of the grid have a vertical wavelength of approximately twice the observed layer height.

Holford & Linden (1999*b*) describe the development of vertical vortices in the lee of eight vertical bars with $b = 0.65$ cm in type (b) experiments. They observe that in experiments with $Re_0 < 140$ and, approximately $1.0 < Fr_0 < 1.9$, the vortices are bent in the x-direction of the grid motion, becoming sinusoidal in the vertical. The effect of bending the vertical vortices is to produce a horizontal component of vorticity in the x-direction, the maximum (positive) and minimum (negative) horizontal components of x-vorticity in each vertical wavelength both tending to overturn isopycnals. This leads to layers with a vertical height half that of the bent vortices.

The possible existence and effect of shear waves is not recognised by Holford & Linden. The agreement of scales of layers and waves supports the conclusion that the mechanism causing the layers is an interaction of the vertical vortices and the internal shear waves generated by the moving vertical grid bars. As noted in § 3.4.1, the internal waves generate two shear layers in each vertical wavelength, one of

https://doi.org/10.1017/jfm.2016.121 Published online by Cambridge University Press

positive horizontal vorticity and one negative. Bending the vertical vortices, these shear layers result in mixed layers of height $h = \lambda_z/2$ or, from (4.5),

$$h/b = \pi Fr_0, \tag{4.6}$$

implying a value of h/b well within the scatter of observed points in figure 5.

What happens when the grid bars reverse their horizontal motion at the two ends of the tank? The conditions at the upper and lower ends of the bars determine the phase of waves and the location of associated shear layers along the vertical bars. The phase can adjust by half a vertical wavelength when the direction of bar motion reverses; the particle motions within the shear layers composing the waves continue to be forced even though the direction of grid motion and wave propagation is reversed at the end of each grid stroke. Since layers are formed by mixing at the levels where the internal wave shear is a positive or negative maximum, the mean horizontal flow induced there by the internal waves is zero; the vertical phase of the horizontal flow induced by the waves is $\pi/2$ out of phase with that of the shear. It is therefore not expected that the layers will be in relative motion. (No examination of the relative mean flow in the layers appears to have yet been made to confirm or refute this conclusion.)

The long times, $(Nt)_1$, required for the formation of layers in the type (*b*) experiments (table 1) are presumably a consequence of the relatively weak forcing of internal waves by the grids. The effect of molecular viscosity, ν, and diffusivity, κ, on the internal shear waves is very small, tending slightly reduce their horizontal phase speed and to damp them by a factor $\exp(-\delta Nt)$, where $\delta = (\nu + \kappa)m^2/2N$ (Ostrovsky & Zaborskikh 1996); δ is of order 10^{-4} for typical values of ν, κ, m and N in the experiments. Residual turbulent motions are relatively weak ahead of the grid when layers are formed, but their dissipative, diffusive and dispersive effects on the internal waves are presently unknown.

4.5. *Boundary-driven layering*

Dr Holford and Professor Linden have provided a copy of a draft referred to in Holford & Linden (1999*a*) as Holford & Linden (1999*b*) that was submitted to 'The Physics of Fluids' but not published. In it they describe how, when $90 < Re_0 < 300$ and $2.7 < Fr_0 < 7.1$, layers develop sequentially over a time period of typically an hour ($Nt \sim 6 \times 10^3$) from the upper and lower boundaries of the laboratory tank in their type (*b*) experiment with $b = 0.65$ cm. This is a parameter regime in which figure 3 indicates that layers are unlikely to be formed in the other type (*b*) experiments. The layer height is $(1–2)U/N$, less than that in (4.2) and (4.3), and therefore indicative of a different form of layer formation. (Williamson 1996, described the local distortion of vortex streets near the ends of a long moving cylinder in an unstratified fluid. Because of buoyancy effects, such distortion is unlikely to be a significant effect in the stratified fluids considered here.)

4.6. *Summary of §§ 4.1–4.5*

Layers in type (*b*) experiments are formed only in conditions in which overturning within the decaying turbulent flow left by one stroke of the moving grid has virtually ceased before the next arrives. The height, h, of layers is consistent with their generation through the bending of vertical wake vortices by internal shear waves moving at the speed of the grid. Once formed, layers may be supported by the PPI mechanism (Holford & Linden 1999*a*).

https://doi.org/10.1017/jfm.2016.121 Published online by Cambridge University Press

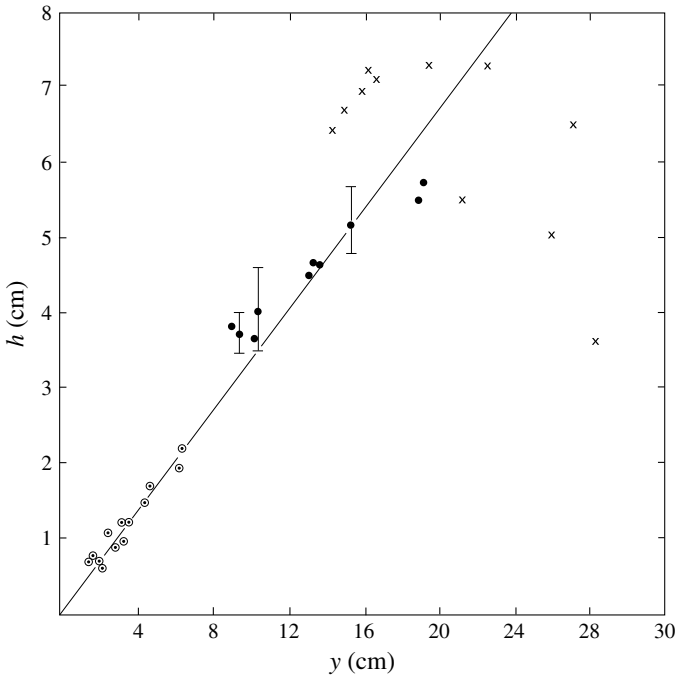


FIGURE 7. The variation in the mean height, h, of the intrusions with the length scale, y. Open circles (○) are points determined by Thorpe (1982, taken from his figure 6*b*) in type (*a*) experiments, and closed circles (●) from Maffioli *et al.* (2014, their figure 15) in type (*c*) experiments using $y = (aM)^{1/4}(U/N)^{1/2}$ where U is the steady grid speed and a the amplitude of grid motion. Points (×) are from Liu *et al.*'s (1987) type (*c*) experiments (see appendix E). The line is $h = 0.34y$.

5. Experiments of type (*c*)

5.1. *The layer height*

In these experiments a grid is moved for a short time through a uniformly stratified layer, producing a turbulent cloud that then collapses. In the experiments by Liu *et al.* (1987) and Maffioli *et al.* (2014) the grid moves through only half of the tank length. As turbulence decays, layers appear as intrusions into the quiescent fluid from the boundary of the turbulent layer. Maffioli *et al.* use a grid of vertical square bars with $b = 0.64$ cm and find

$$h/b = 2.4Fr_0^{0.313} \tag{5.1}$$

is a best fit to data, with $16 < Fr_0 < 74$ (or approximately 5.7 cm $< h <$ 9 cm). As shown in figure 5, (5.1) differs from the linear relationships of the type (*b*) experiments both in shape and in their ranges; the range of $Fr_0 = U/Nb$ is approximately 0.4–1.8 in the type (*b*) experiments, much less than the range of Fr_0 in Maffioli *et al.*'s experiments. Considerable scatter of points is found in figure 6 where h/b is plotted versus $U/Nb\,(= Fr_0)$ using data from the type (*a*) experiments of Thorpe (1982) and Browand *et al.* (1987), the type (*c*) experiments of Liu *et al.* and Maffioli *et al.*, and the type (*b*) experiments (shown as the dashed line $h/b = 3.03U/Nb$ taken from figure 5). No universal relation between h/b and U/Nb (or y/b) appears to exist; the scaling of the layer heights depends on the different processes through which layers are formed or sustained in each type of experiment.

https://doi.org/10.1017/jfm.2016.121 Published online by Cambridge University Press

Maffioli *et al.* argue that turbulent mixing causes the formation of mixed packets of fluid within the turbulent cloud that collapse producing the laterally spreading intrusions, much as described in § 3.3 in relation to the type (*a*) experiments. There is a further similarity: if the factor $a\omega$ in the expression (3.4) for y is replaced by the steady grid speed U in Maffioli *et al.*'s type (*c*) laboratory experiments, there is a fair agreement between Maffioli *et al.*'s observed intrusion heights with those of the type (*a*) experiments, as shown in figure 7. Appendix E is a note explaining how points in in figures 6 and 7 from Liu *et al.* (1987) are determined.

The similarity of the scale of h in type (*c*) transient turbulence experiments with that found in the type (*a*) maintained mixing experiments lends support to the conclusions of § 3.2.1 that layers are formed, and their vertical scale is determined, at a very early stage of grid motion.

6. Discussion and conclusions

The best quantified measures of the layers formed in the turbulent flow generated by a grid moving through a uniformly stratified fluid in a laboratory tank is their height, h, and its variation with the forcing parameters and with the initial buoyancy frequency of the fluid. In experiments of type (*a*) and (*c*) in which only part of the tank is stirred, the layers appear as intrusions with a vertical scale $h = \gamma y$, with $\gamma \approx 0.33$ and $y = (aM)^{1/4}(a\omega/N)^{1/2}$ (§ 3.1, and § 5.1 taking $a\omega = U$). In type (*b*) experiments layers form within the turbulent fluid with scale $h/b \approx \pi Fr$ with $Fr = U/Nb$ (§ 4.3). These layer scales are distinct (e.g. they have different variations with N) and it therefore does not appear that the intrusions in type (*a*) experiments are a consequence of the horizontal spreading of layers formed (but perhaps unrecognised in the experiments) within the turbulent region by the same mechanism, the bending of vortices, as in the type (*b*) experiments. Rather the layers in type (*a*), and the type (*c*), experiments appear to be formed as a consequence of the collapse and spread of regions mixed by large overturns within the turbulent region soon after turbulence is first generated.

In none of the experiments are the layers demonstrably a result of zigzag instability.

In type (*a*) experiments the local Froude number, Fr, characterises the variation of the state of turbulence with distance from its generation by the moving grid; the vertical scale of intrusions, h, is equal to the local Ozmidov length scale in the turbulent region where $Fr \sim 1.85$, at a distance from the grid of approximately 0.39 times that of the edge of the turbulent region (table 4). At the outer edge of the turbulent region ($x = \eta$), Fr is found to be approximately 0.28. This value is uncertain, however, because it depends on the unreliable estimates of w and l given by (3.1) and (3.2) in a region affected by stratification and therefore beyond their strict range of validity. The leading internal waves propagating ahead of the intrusions have a vertical wavelength of approximately $2h$, twice the thickness of the layers; waves of smaller vertical scale do not travel fast enough to advance more rapidly than the intrusions when they are first observed emerging from the turbulent region (§ 3.4.4).

Overturning has generally ceased within the time periods between successive mixing by a grid in those type (*b*) experiments of table 1 in which layers are observed (§ 4.2); the process generating layers operates in conditions in which the residual turbulence is relatively weak. Internal shear waves with a horizontal group velocity that matches the speed of the moving grids have a vertical wavelength of approximately $2h$ (§ 4.4). The layers consequently appear to be generated as a result of a mixing mechanism described by Holford & Linden (1999*a*,*b*): vertical vortices shed by the mixing bars are bent by the shear layers within the internal waves, resulting in horizontal

https://doi.org/10.1017/jfm.2016.121 Published online by Cambridge University Press

x-components of vorticity that drive overturning and lead to mixing. Two shear layers, one positive, the other negative, are present in each vertical wavelength of the internal waves and hence the layer height is approximately half the vertical wavelength. The generation process is weak because of the relatively slow production of the internal waves of vertical scale $2h$ by the vertical grid bars and the damping effect of residual turbulence; layers therefore form only after relatively long periods of time. Although Holford & Linden (1999*a*) conclude that layers cannot be formed as a result of the PPI mechanism in type (*b*) experiments, once they are formed layers can be supported by PPI.

There is a remarkable contrast in the relationship of layers and internal shear waves in the experiments. In type (*a*) and (*c*) experiments internal waves are generated by layers intruding from the turbulent region into the quiescent stratified region. In experiments of type (*b*) internal waves drive and dictate the height of the layers; layers are generated as a consequence of vortex bending by internal waves.

The finding that the layer height in the type (*b*) experiments is half that of the internal shear waves that are stationary relative to the moving grid prompts a re-examination of the similar relation between waves and intrusions in the type (*a*) experiments. Rather than being generated by the intrusions, might the internal shear waves provide a mechanism that contributes to mixing in the intruding layers? The only direct evidence appears to be that provided by Browand *et al.*'s (1987) figure 15(*b*). It shows the horizontal displacements produced by the internal waves in vertical lines of dye in the uniformly stratified quiescent fluid before the arrival of the intrusive motions. As well as having a scale half that of the internal waves, the intrusions often appear at levels of maximum positive or negative wave shear as would be expected if the shear leads to the bending of vertical vortices and contributes to mixing in the intrusions. The evidence is however insufficient to be conclusive but the absence of vortices in the quiescent fluid argues against vortex bending as a contribution to layering. The regular vertical periodicity of the intrusions in the type (*a*) experiments remains unexplained although some interaction of internal waves and intrusions appears likely.

The DNS experiments listed in table 2 differ physically from the grid mixing experiments, particularly those of type (*c*). In the latter, turbulence is initiated by a grid over a finite period of time, typically non-dimensional times $Nt = 2.5$–10.5 in laboratory experiments by Liu *et al.* (1987) or $Nt = 7.7$ in those of Maffioli *et al.* (2014), rather than instantaneously as in the numerical studies. Moreover the parameter ranges differ as can be seen by comparing tables 1 and 2. If, as seems possible, the layers produced by moving grids in the laboratory experiments are generated early in the mixing process, and their properties (e.g. h) depend on the grid scales (e.g. M and b) it is unlikely that the numerical experiments – although valuable in describing the collapse of turbulence, consequent layer formation and internal wave generation – faithfully reproduce all the processes leading to the formation of layers generated by grids in the laboratory experiments. In particular, the vortices generated by moving grids are not represented in the numerical experiments. Few quantitative comparisons of numerical and laboratory experiments have been made, an exception being the radiation of internal waves at their group velocity. Maffioli *et al.*, however, report comparison of the thickness of intrusions in two numerical experiments with the same integral length scale, l_0, but different initial Froude numbers, Fr_0, the thickness being greater in the experiment with the higher Fr_0. This is in accord with the results of the type (*a*) experiments: these lead to $h = \gamma y = \gamma (aM)^{1/4}(a\omega/N)^{1/2} \sim \gamma (aM)^{1/4}(U/N)^{1/2}$ or $h \sim \gamma (aMl_0^2)^{1/4} Fr_0^{1/2}$; i.e. an increase in h with Fr_0 as found numerically, but

https://doi.org/10.1017/jfm.2016.121 Published online by Cambridge University Press

further comparison is desirable. It follows, however, that the type (*a*) experiments have $h/b \sim Fr_0^{1/2}$. Although the $Fr_0^{1/2}$ relation differs from (5.1), i.e. that determined from the type (*c*) experimental data $h/b \sim Fr_0^{0.313}$, figure 7 suggests that the type (*c*) data is reasonably well fitted by the $Fr_0^{1/2}$ relation applicable to type (*a*) experiments. The linear dependence (4.4) of h/b on Fr_0 in the type (*b*) experiments is further supportive evidence of the fundamental difference between the type (*a*) and (*c*) experiments and those of type (*b*).

Many of the ideas advanced on the basis of laboratory experiments to explain the scale and formation of layers disregard, as we have done here, features that may well become important, particularly the three-dimensional spreading of mixed regions within the turbulent flow, the generation of pancake-like vortical modes explored by Fincham, Maxworthy & Spedding (1996) and Praud *et al.* (2005) and the limiting effects of side walls. The laboratory experiments provide largely two-dimensional information about the field of motion outside the turbulent region and of the intrusions and internal waves, but relatively little about the processes within a sustained or collapsing turbulent region (although laboratory methods are now available to make relevant microscale measurements of density and velocity). The numerical studies have the potential to explore motion and mixing both outside the turbulent region and within it, to examine relations between the mean size of the intrusion height, h, the overturning eddies and L_O, and to investigate the formation and maintenance of the intruding layers in three dimensions. Further carefully designed laboratory and numerical experiments will usefully shed further light on the interactions between turbulence, stratification and internal waves.

Acknowledgements

I am most grateful to Dr A. Maffioli and Professor P. Linden for advice and comment. Professor Linden and Dr J. Holford generously provided a copy of Holford & Linden (1999*b*) and a draft of their work on boundary-driven layering referred to in § 4.5. I thank anonymous referees for their many very helpful suggestions.

Appendix A. Values of C and β and u/w

Hopfinger & Toly (1976) investigate w and l with grids of mesh size, $M = 5$ and 10 cm, and square bar widths, $b = 0.2M$. A value of $C = 0.25 \pm 0.05$ fits experimental data with a stroke, $s = 2a$, of 1–9 cm. Values of β (determined from their figure 8) vary from 0.17 (M = 10 cm, s = 4 cm) to 0.33 (M = 10 cm, s = 9 cm). When $M = 5$ cm and $b = 1$ cm, the non-dimensional coefficients, C and β, are found by Hopfinger & Linden (1982) to depend on s: $C = 0.2$ (for $s = 1$, 2.4 cm) and $C = 0.3$ ($s = 4$ cm), while $\beta = 0.1$ ($s = 1$ cm), 0.17 ($s = 2.4$ cm) and 0.25 ($s = 4$ cm). De Silva & Fernando (1998) find $C \sim 0.15$ and $\beta \sim 0.1$ in their experiments with an oscillating (horizontal) grid with square bars having $M = 4.76$ cm and $b = 1$ cm, and when 0.4 cm $\leqslant s \leqslant$ 1.5 cm (but mostly $s = 0.85$ cm). (Browand *et al.* (1987) adopt the extrapolated values $C = 0.29$ and $\beta = 0.26$ for the analysis of their experiments with a vertical square grid with $M = 5$ cm, $b = 1$ cm, as used by Hopfinger & Toly, and $s \sim 4.5$ cm.)

Hopfinger & Toly find that the r.m.s. turbulent vertical fluctuations, u, are approximately $1.05w$ when M = 5 cm, s = 4 cm and $x \gtrsim 1.5M$, whereas in their experiments Hopfinger & Linden find $u \sim 1.25w$ for $x \gtrsim M$, and De Silva & Fernando find $u \sim 1.3w$.

https://doi.org/10.1017/jfm.2016.121 Published online by Cambridge University Press

x/η	h/L_O	I	Fr
0.591–0.599	2.31–2.38	200	0.776–0.800
0.952–0.964	5.98–6.15	30	0.300–0.310

TABLE 6. Values obtained from Browand *et al.*'s (1987) type (*a*) experiments using $C = 0.29$, $\beta = 0.26$, $\alpha = 1.34$, $\gamma = 0.34$ and listed in order of increasing x/η through the turbulent region. ($x/\eta = 1$ is the location of its mean boundary.)

Appendix B. The local buoyancy Reynolds number, I, as a similarity parameter

The parameter, I_0, shown in table 1 and defined in § 1.2 is a measure of the buoyancy Reynolds number, associated with the grid motion in the various experiments. Using (3.1) and (3.2), the local buoyancy Reynolds number, $I = \varepsilon/(\nu N^2)$, is equal to

$$I = 2^{3/2} C^3 y^6 N/(\pi^3 x^4 \beta \nu), \tag{B 1}$$

if $\varepsilon = w^3/l$. Gargett, Osborn & Nasmyth (1984) find that turbulent motion is isotropic if $I > 200$ (or equivalently $L_O/L_K \sim 53$, allowing there to be a substantial spectral range between the Ozmidov overturning scale, L_O, and the Kolmogorov dissipation scale, L_K). For smaller I motion is anisotropic, vertical displacements being constrained by stratification. Gibson (1980) proposes that the condition $I \geqslant 30$ is required for the existence of active turbulence with wavelength λ in the range $1.2Lo \geqslant \lambda \geqslant 15L_K$, with remnant 'fossil' turbulence at lower values of I. We consider whether $I = I_c \sim 30$ or 200 provide values that may characterise boundaries for the collapse of active turbulence or for isotropic turbulence, largely unaffected by stratification, in the three experiments of type (*a*). If valid, these critical values should be found at similar values of x/η and h/L_O in all experiments of type (*a*).

At $I = I_c$, from (B 1):

$$x = x_{cI} = [2^{3/2} C^3 y^6 N/(I_c \pi^3 \beta \nu)]^{1/4}. \tag{B 2}$$

At this distance from the grid, using (3.7):

$$L_O = (I_c \nu/N)^{1/2}. \tag{B 3}$$

These equations, with (3.5) and (3.6), are used to find expressions of x/η and h/L_O at $I = 30$ and 200 in terms of C and β. Values in Browand *et al.*'s (1987) experiment (where C and β are known) are shown in table 6. It proves impossible, whatever values of the unknown C and β are chosen for Thorpe's (1982) and Ivey & Corcos' (1982) experiments, to match the values of x/η and h/L_O in this table. We conclude that the local buoyancy Reynolds number, I, is not a parameter that characterizes the local turbulent flow in all the three experiments of type (*a*).

Appendix C. Waves generated by density currents at the upper and lower boundaries

The frequency, σ, of internal gravity waves with horizontal and vertical wavenumbers, k and m, respectively, in a fluid of uniform buoyancy frequency, N, is given by

$$\sigma^2 = k^2 N^2/(k^2 + m^2), \tag{C 1}$$

https://doi.org/10.1017/jfm.2016.121 Published online by Cambridge University Press

and the horizontal and vertical group speeds, found by differentiation with respect to k and m, respectively, are

$$c_{gx} = \pm m^2 N/(k^2+m^2)^{3/2} \quad \text{and} \quad c_{gz} = \pm kmN/(k^2+m^2)^{3/2}, \tag{C 2a,b}$$

respectively (e.g. see Thorpe 2010). The horizontal velocity, c_{gx}, decreases as k increases and equals N/m at $k=0$; $\max(c_{gx}) = N/m$. (From (C 1) the horizontal phase speed, σ/k, of these waves with $k=0$ is also equal to N/m.) The wave modes satisfying conditions of zero vertical velocity at the top and bottom of the tank have $m = n\pi/H$, where n is a positive integer, and so $\max(c_{gx}) = NH/\pi$ (the speed of the lowest mode, when $n=1$).

We suppose that density currents at the top or bottom boundary of a tank generate internal waves that advance ahead of the currents. The time taken for internal waves generated by the gravity currents to reach the end of a tank of length L is at least $T_x = L\pi/NH$. But how long is it before the waves extend over the depth of the tank?

The maximum vertical group velocity, $\max(c_{gz}) = 2N/(3k\sqrt{3})$, is found when $m = k/\sqrt{2}$. If the horizontal wavelength of waves generated by the density currents is $\lambda_x = L/2$, then $\max(c_{gz}) = NL/(6\pi\sqrt{3})$. (A smaller λ_x gives bigger k and smaller c_{gz}.) The time, T_z, to reach the bottom of the tank and to establish the lowest, $n=1$, mode is at least $6\pi H\sqrt{3}/NL$.

Values of H and L in experiments by Browand *et al.* (1987) are 50 and 100 cm (or, in a second tank, 150 cm and 120 cm), respectively, with some uncertainty concerning the location of the grid. Those in Thorpe's (1982) experiment are 30.5 cm and 20.3 cm, respectively. These give $NT_x = 6.3$ and $NT_z = 16.3$ (or 2.5 and 40.8), respectively, in Browand *et al.*'s experiments, and (2.1) and (49.1), respectively, in Thorpe's.

It consequently appears unlikely that the density currents travelling at or near the upper and lower boundaries of the tanks in these laboratory experiments have much effect on the mid-depth intrusions before non-dimensional times exceeding 16.

Appendix D. Internal shear waves generated by the intrusions

The horizontal velocities, u', of the intrusions at the boundary, $x=0$, of the turbulent region can be expressed as

$$u'(x=0) = \left[\sum_{m=1}^{m=\infty} u_m \cos(2m\pi z/h) + \sum_{n=2} v_n \cos(2\pi z/nh)\right] \cos\sigma t, \tag{D 1}$$

in the limit as the non-dimensional frequency, σ/N, tends to zero, where m and n are positive integers. The first term with $m=1$ in the first summation represents the principal near-sinusoidal intrusions of vertical separation, h. The higher values of m in the summation represent displacements of their shape from sinusoidal. The second summation is over $n = 2, 4, 8, \ldots$ to $2^L = H/2h$, where L is an integer. It represents variations in the vertical of the relative amplitude of the intrusions. The form of this second summation is chosen, for simplicity, to make $2\pi z/nh$ equal to $\pm\pi$ at $n = 2^L$ and $z = \pm H/2$, and consequently to allow the vertical velocity, w', in the solution below to satisfy the boundary condition, $w' = 0$ at $z = \pm H/2$. In the experiments, H/h is in the range 13–61 so L is typically 3–5. Since the intrusions are dominated by those with height, h, $v_n (n \geqslant 2)$ is much less than u_1.

https://doi.org/10.1017/jfm.2016.121 Published online by Cambridge University Press

Following the wave maker theory in Thorpe (1968), a linear solution for the resulting internal waves with velocity components (u^*, w^*) which satisfies (D 1) and the condition of zero vertical velocity at the horizontal boundaries at $z = \pm H/2$ is

$$u^* = \sum_{m=1}^{m=\infty} u_m \cos(2m\pi z/h)\cos(k_m x - \sigma t) + \sum_{n=2} v_n \cos(2\pi z/nh)\cos(k_n x - \sigma t) \qquad (D\,2)$$

and

$$w^* = \sum_{m=1}^{m=\infty} (u_m k_m h/2m\pi)\sin(2m\pi z/h)\sin(k_m x - \sigma t) + \sum_{n=2} (v_n k_n hn/2\pi)\sin(2\pi z/nh)\sin(k_n x - \sigma t), \qquad (D\,3)$$

where k_m and k_n are horizontal wavenumbers satisfying the dispersion relations

$$k_m^2 = \sigma^2(2m\pi/h)^2/(N^2 - \sigma^2) \quad \text{and} \quad k_n^2 = \sigma^2(2\pi/nh)^2/(N^2 - \sigma^2). \qquad (D\,4a,b)$$

Each of the u^* and w^* components of velocity in (D 2) and (D 3), $u_m \cos(2m\pi_z/h)\cos(k_m x - \sigma t)$ and $(u_m k_m h/2m\pi)\sin(2m\pi z/h)\sin(k_m x - \sigma t)$ (or $v_n \cos(2\pi z/nh)\cos(k_n x - \sigma t)$ and $(v_n k_n nh/2\pi)\sin(2\pi nz/H)\sin(k_n x - \sigma t)$) represent waves with horizontal wavenumber k_m (or k_n, respectively) that, individually, are exact solutions of the equations of motion, nonlinear terms being identically zero and each vertical component satisfying $w^* = 0$ at $z = \pm H/2$. Resonant interactions between waves of different wavenumbers are possible (Martin, Simmons & Wunsch 1972), but being relatively slow are unlikely to lead to any substantial changes in wave propagation in the length of the tank or during the time before waves reflect from the end walls. Both $k_m h$ and $k_n h$ tend to zero as σ/N tends to zero.

The horizontal velocity of the shear waves found from (D 2) as σ/N, $k_m h$ and $k_n h$ all tend to zero is $u^* = \sum_{m=1}^{m=\infty} u_m \cos(2m\pi z/h) + \sum_{n=2} v_n \cos(2\pi z/nh)$. The horizontal group velocities of the wave components given in appendix C are

$$c_{gxm} = Nh/2m\pi \quad \text{and} \quad c_{gxn} = Nhn/2\pi, \qquad (D\,5a,b)$$

respectively. If, as observed (§ 3.4.4), the intrusion speed, approximately u_1, is in the range (0.19–0.32)Nh, the ratio c_{gxm}/u_1 equals $1/[2m\pi(0.19\text{–}0.32)](n \geqslant 1) <$ (0.50–0.84), for all $n \geqslant 1$ in the first summation; the group velocity of waves resulting from the non-sinusoidal components of the perturbation resulting from intrusions – and of the intrusions themselves – is smaller than the speed at which the intrusion advances. If the waves represented by the second summation propagate ahead of the intrusions (i.e. $c_{gxn} > u_1$), then using (D 5), the integer, n, must exceed $2\pi(0.19\text{–}0.32) = (1.19\text{–}2)$. Only waves with $n \geqslant 2$ and therefore with vertical scale equal to or exceeding $2h$ can propagate ahead of the intrusions.

Equating the decreasing speed of the front of intrusions given by (3.8) to the group speed, $Nh/2\pi$, of waves with vertical scale h, we find that waves of scale h may eventually be generated but only if $Nt > 41$ in Browand *et al.*'s experiments or $Nt > 12.4$ in Thorpe's, times after the intrusions have emerged from the turbulent region.

https://doi.org/10.1017/jfm.2016.121 Published online by Cambridge University Press

Appendix E. Liu *et al.*'s (1987) experiments

Figures 6 and 7 contain points from Liu *et al.* (1987). In the description of their experiments with a grid of vertical square bars with $b = 1.27$ cm, individual estimates of h are not provided, but have been inferred from their table 1 with the value of the integral length scale, l, taken from their figure A1 as approximately 1 cm at $x/M = 0$. With $a\omega = U$ in the expression for y, a mean value $\gamma = 0.37 \pm 0.17$ is obtained in a relation between h and y, h lying between approximately 3.6 and 11.8 cm. Liu *et al.*'s points in figures 6 and 7 have considerable scatter but, given the uncertainty in l and in measuring h, the coefficient of proportionality, γ, is in reasonable accord with the values in the type (a) experiments, i.e. approximately 0.33 ± 0.01. The mean values of h/b, y and U/Nb are 5.8, 22 and 19.9, respectively, leading to points lying close to the fits, (5.1) and $h = 0.34y$, of figures 6 and 7, and indicating the general consistency of Liu *et al.*'s experiments with those of Maffioli *et al.* Liu *et al.* also find values of h in excess of the Ozmidov length scale, L_O, by a factor of approximately 10, see § 3.2.2, but there is uncertainty both in the way, and about where, L_O is estimated.

REFERENCES

ALFORD, M. H. & GREGG, M. C. 2001 Near-inertial mixing: modulation of shear, strain and microstructure at low latitude. *J. Geophys. Res.* **106**, 16947–16968.

AUGIER, P. & BILLANT, P. 2011 Onset of secondary instabilities on the zigzag instability in stratified fluids. *J. Fluid Mech.* **682**, 120–131.

BAINES, P. G. 1995 *Topographic Effects in Stratified Flows*. p. 482. Cambridge University Press.

BAINES, P. G. 2001 Mixing by flows down gentle slopes into stratified environments. *J. Fluid Mech.* **443**, 237–270.

BALMFORTH, N. J., LLEWELLYN SMITH, S. G. & YOUNG, W. R. 1998 Dynamics of interfaces and layers in a stratified turbulent fluid. *J. Fluid Mech.* **355**, 329–358.

BILLANT, P. & CHOMAZ, J.-M. 2000 Experimental evidence for a new instability of a vertical columnar vortex pair in a strongly stratified fluid. *J. Fluid Mech.* **418**, 167–188.

BOLSTER, D., HANG, A. & LINDEN, P. F. 2008 The front speed of intrusions into a continuously stratified medium. *J. Fluid Mech.* **594**, 369–377.

BOSCO, M. & MEUNIER, P. 2014 Three-dimensional instabilities of a stratified cylinder wake. *J. Fluid Mech.* **759**, 149–180.

BRITTER, R. E., HUNT, J. C. R., MARSH, G. L. & SNYDER, W. H. 1983 The effects of stable stratification on turbulent diffusion and the decay of grid turbulence. *J. Fluid Mech.* **127**, 27–44.

BROWAND, F. K., GUYOMAR, D. & YOON, S.-C. 1987 The behaviour of a turbulent front in a stratified fluid: experiments with an oscillating grid. *J. Geophys. Res.* **92** (C5), 5329–5341.

DELONCLE, A., BILLANT, P. & CHOMAZ, J.-M. 2008 Nonlinear evolution of the zigzag instability in stratified fluids: a shortcut on the route to dissipation. *J. Fluid Mech.* **599**, 229–230.

DELONCLE, A., BILLANT, P. & CHOMAZ, J.-M. 2011 Three-dimensional stability of vortex arrays in a stratified and rotating fluid. *J. Fluid Mech.* **678**, 482–510.

DE SILVA, I. P. D. & FERNANDO, H. J. S. 1998 Experiments on collapsing turbulent regions in stratified fluids. *J. Fluid Mech.* **358**, 29–60.

DIAMESSIS, P. J. & NOMURA, K. K. 2004 The structure and dynamics of overturns in stably stratified homogeneous turbulence. *J. Fluid Mech.* **499**, 197–229.

DICKEY, T. D. & MELLOR, G. L. 1980 Decaying turbulence in neutral and stratified fluids. *J. Fluid Mech.* **99**, 13–32.

DILLON, T. M. 1982 Vertical overturns: a comparison of Thorpe and Ozmidov length scales. *J. Phys. Oceanogr.* **87**, 9601–9613.

FERRON, B., MERCIER, H., SPEER, K., GARGETT, A. & POLZIN, K. 1998 Mixing in the Romanche fracture zone. *J. Phys. Oceanogr.* **28**, 1929–1945.

https://doi.org/10.1017/jfm.2016.121 Published online by Cambridge University Press

FINCHAM, A. M., MAXWORTHY, T. & SPEDDING, G. R. 1996 Energy dissipation and vortex structure in freely decaying, stratified grid turbulence. *Dyn. Atmos. Oceans* **23**, 155–169.

GARGETT, A., OSBORN, T. R. & NASMYTH, P. W. 1984 Local isotropy and the decay of turbulence in a stratified fluid. *J. Fluid Mech.* **144**, 231–280.

GIBSON, C. H. 1980 Fossil temperature, salinity, and vorticity turbulence in the pcean. In *Marine Turbulence* (ed. J. Nihoul), Elsevier Oceanography Series, pp. 221–257. Elsevier.

HOLFORD, J. M. & LINDEN, P. F. 1999*a* Turbulent mixing in a stratified fluid. *Dyn. Atmos. Oceans* **30**, 173–198.

HOLFORD, J. M. & LINDEN, P. F. 1999*b* The development of layers in a stratified fluid. In *Mixing and Dispersion in Stably Stratified Flows. Proceedings of 5th IMA Conference on Statified Flows, University of Dundee, Scotland*, pp. 165–179. Oxford University Press.

HOPFINGER, E. J. & LINDEN, P. F. 1982 Formation of thermocline in zero-mean-shear turbulence subjected to a stabilizing buoyancy flux. *J. Fluid Mech.* **114**, 157–173.

HOPFINGER, E. J. & TOLY, J. A. 1976 Spatially decaying turbulence and its relation to mixing across density interfaces. *J. Fluid Mech.* **78**, 155–175.

INALL, M. 2009 Internal wave induced dispersion and mixing on a sloping boundary. *Geophys. Res. Lett.* **36**, L05604.

ITSWEIRE, E. C. 1984 Measurements of vertical overturns in a stably stratified turbulent flow. *Phys. Fluids* **27**, 764–766.

ITSWEIRE, E. C., HELLAND, K. N. & VAN ATTA, C. W. 1986 The evolution of grid-generated turbulence in a stably stratified fluid. *J. Fluid Mech.* **162**, 299–338.

IVEY, G. N. & CORCOS, G. M. 1982 Boundary mixing in a stratified fluid. *J. Fluid Mech.* **121**, 1–26.

LAZIER, J. N. R. 1973 Temporal changes in some fresh water temperature structures. *J. Phys. Oceanogr.* **3**, 226–229.

LIU, Y. N., MAXWORTHY, T. & SPEDDING, G. R. 1987 Collapse of a turbulent front in a stratified fluid. 1: nominally two-dimensional evolution in a narrow tank. *J. Geophys. Res.* **92** (C5), 5427–5433.

MAFFIOLI, A., DAVIDSON, P. A., DALZIEL, S. B. & SWAMINATHAN, N. 2014 The evolution of a stratified turbulent cloud. *J. Fluid Mech.* **739**, 229–253.

MANINS, P. C. 1976 Intrusions into a stratified fluid. *J. Fluid Mech.* **74**, 547–560.

MARTIN, J. E. & REHMANN, C. R. 2006 Layering in a flow with diffusively stable temperature and salinity stratification. *J. Phys. Oceanogr.* **36**, 1457–1470.

MARTIN, S., SIMMONS, W. & WUNSCH, C. 1972 The excitation of resonant triads by single internal waves. *J. Fluid Mech.* **53**, 17–44.

MATER, B. D., SCHAAD, S. M. & VENAYAGAMOORTHY, S. K. 2013 Relevance of the Thorpe Lengthscale in stably stratified turbulence. *Phys. Fluids* **25**, 076604.

MAURIER, B. D. & LINDEN, P. F. 2014 Intrusion-generated waves in a linearly stratified fluid. *J. Fluid Mech.* **752**, 282–295.

MAXWORTHY, T., LEILICH, J., SIMPSON, J. & MEIBURG, E. H. 2002 The propagation of a gravity current in a linearly stratified fluid. *J. Fluid Mech.* **453**, 371–394.

MCEWAN, A. D. & BAINES, P. G. 1974 Shear fronts and an experimental stratified shear flow. *J. Fluid Mech.* **63**, 257–272.

MEUNIER, P. 2012 Stratified wake of a tilted cylinder. Part 1. Suppression of a von Kármán vortex street. *J. Fluid Mech.* **699**, 174–197.

OSTROVSKY, L. A. & ZABORSKIKH, D. V. 1996 Damping of internal gravity waves by small-scale turbulence. *J. Phys. Oceanogr.* **26**, 388–397.

OTHEGUY, P., CHOMAZ, J.-M & BILLANT, P. 2006 Elliptic and zigzag instabilities on co-rotating vertical vortices in a stratified fluid. *J. Fluid Mech.* **553**, 253–272.

PARK, Y.-G., WHITEHEAD, J. A. & GNANADESKIAN, A. 1994 Turbulent mixing in stratified fluids: layer formation and energetic. *J. Fluid Mech.* **279**, 279–311.

PETERS, H., GREGG, M. C. & TOOLE, J. M. 1988 On the parametrization of equatorial turbulence. *J. Geophys. Res.* **93**, 1199–1218.

https://doi.org/10.1017/jfm.2016.121 Published online by Cambridge University Press

PHILLIPS, O. M. 1972 Turbulence in a strongly stratified fluid – is it unstable? *Deep-Sea Res.* **19**, 79–81.

POSMENTIER, E. S. 1977 The generation of salinity finestructure by vertical diffusion. *J. Phys. Oceanogr.* **7**, 298–300.

PRAUD, O., FINCHAM, A. M. & SOMMERIA, J. 2005 Decaying grid turbulence in a strongly stratified fluid. *J. Fluid Mech.* **522**, 1–33.

RIEDINGER, X., LE DIZÈS, S. & MEUNIER, P. 2011 Radiative instability of the flow around a rotating cylinder in a stratified fluid. *J. Fluid Mech.* **672**, 130–146.

RUDDICK, B. R., MCDOUGALL, T. J. & TURNER, J. S. 1989 The formation of layers in a uniformly stirred density gradient. *Deep-Sea Res.* **36**, 597–609.

SMYTH, W. D., ZAVIALOV, P. O. & MOUM, J. N. 1997 Decay of turbulence in the upper ocean following sudden isolation from surface forcing. *J. Phys. Oceanogr.* **27**, 810–822.

SNOW, K. & SUTHERLAND, B. R. 2014 Particle-laden flow down a slope in uniform stratification. *J. Fluid Mech.* **755**, 251–273.

STANSFIELD, K., GARRETT, C. & DEWEY, R. 2001 The probability distribution of the Thorpe displacement within overturns in Juan de Fuca Strait. *J. Phys. Oceanogr.* **31**, 3421–3434.

STAQUET, C. & GODEFERD, F. S. 1998 Statistical modelling and direct numerical simulations of decaying stably stratified turbulence. Part 1. Flow energetics. *J. Fluid Mech.* **360**, 295–340.

THORPE, S. A. 1968 On the shape of progressive internal waves. *Phil. Trans. R. Soc. Lond.* A **263**, 563–614.

THORPE, S. A. 1982 On the layers produced by rapidly oscillating a vertical grid in a uniformly stratified fluid. *J. Fluid Mech.* **124**, 391–409.

THORPE, S. A. 1998 Some dynamical effects of the sloping sides of lakes. In *Physical Processes in Lakes and Oceans* (ed. J. Imberger), Coastal and Estuarine Studies, ch. 31, pp. 441–460. AGU.

THORPE, S. A. 1999 On internal wave groups. *J. Phys. Oceanogr.* **29**, 1085–1095.

THORPE, S. A. 2010 The relation between the duration and shape of internal wave groups. *J. Mar. Res.* **68**, 63–95.

TURNER, J. S. 1973 *Buoyancy Effects in Fluids*. p. 367. Cambridge University Press.

VENAYAGAMOORTHY, S. K. & STRETCH, D. D. 2006 Lagrangian mixing in decaying stably stratified turbulence. *J. Fluid Mech.* **564**, 197–226.

WAITE, M. L. & SMOLARKIEWICZ, P. K. 2008 Instability and breakdown of a vertical vortex pair in a strongly stratified fluid. *J. Fluid Mech.* **606**, 239–273.

WILLIAMSON, C. H. K. 1996 Vortex dynamics in the cylinder wake. *Annu. Rev. Fluid Mech.* **28**, 477–539.

WUNSCH, S. & KERSTEIN, A. 2001 A model for layer formation in stably stratified turbulence. *Phys. Fluids* **13** (3), 702–712.

XIANG, X., MADISON, T. J., SELLAPPAN, P. & SPEDDING, G. R. 2015 The turbulent wake of a towed grid in a stratified fluid. *J. Fluid Mech.* **775**, 149–177.

YIM, E. & BILLANT, P. 2015 On the mechanism of the Gent-McWilliams instability of a columnar vortex in stratified rotating fluids. *J. Fluid Mech.* **780**, 5–44.

https://doi.org/10.1017/jfm.2016.121 Published online by Cambridge University Press